



Contents lists available at ScienceDirect

Arabian Journal of Chemistry

journal homepage: www.ksu.edu.sa

Terbium metal–organic frameworks for the efficient removal of tartrazine food dye from aquatic systems: Thermodynamics, kinetics, isotherm, and box-behnken design optimization

Omaymah Alaysuy^a, Abdullah Ali A. Sari^b, Albandary Almahri^c, Kamelah S. Alrashdi^d, Ibrahim S.S. Alatawi^a, Meshari M. Aljohani^a, Ali Sayqal^e, Nashwa M. El-Metwaly^{e,f,*}

^a Department of Chemistry, College of Science, University of Tabuk, Tabuk, Saudi Arabia

^b Department of Chemistry, University College in Al-Jamoum, Umm Al-Qura University, 21955 Makkah, Saudi Arabia

^c Department of Chemistry, College of Science and Humanities in Al-Kharj, Prince Sattam Bin Abdulaziz University, Al-Kharj 11942, Saudi Arabia

^d Department of Chemistry, Al-Qunfudah University College, Umm Al-Qura University, Al-Qunfudah 1109, Saudi Arabia

^e Department of Chemistry, Faculty of Science, Umm Al Qura University, Makkah 24230, Saudi Arabia

^f Department of Chemistry, Faculty of Science, Mansoura University, Mansoura, Egypt

ARTICLE INFO

Keywords:

Tartrazine food dye
Adsorption isotherm
Adsorption kinetics
Tb-MOF
Box–Behnken Design

ABSTRACT

The elimination and removal of the yellow food coloring tartrazine dye E-102 (TZ) from aqueous solutions was conducted using stacked nanorods made of Terbium metal–organic frameworks (Tb-MOF). The adsorbent was assessed using various methods including FTIR, BET, XRD, XPS, SEM, and TEM. The results showed that the surface area decreased from 1123.07 to 762.8 m²·g⁻¹, the pore volume reduced from 4.02 to 2.6 cc/g, and the pore size decreased from 7.8 to 3.2 nm after adsorption. The reduction in surface area, pore volume, and pore size post-TZ dye adsorption indicates that some of the adsorption mechanisms took place through the pores of the adsorbent. Examined the impact of temperature, pH, initial dye concentration, and contact time on the removal of TZ dye. The adsorption of TZ was found to conform to the Langmuir isotherm and pseudo-second-order kinetic model. The maximum adsorption capacity for TZ was determined to be 817.63 mg/g. The resulting pH_{ZPC} value of 5.36 indicates that adsorption of anionic dyes, such as TZ dye, is advantageous at pH levels below 5.36. Moreover, the adsorption process exhibited an adsorption energy of 23.78 kJ/mol, suggesting the presence of a chemisorption mechanism. The thermodynamic parameters calculated indicate that the adsorption processes are both spontaneous and endothermic. It is advisable to utilize the Tb-MOF adsorbent for a total of five cycles, as the adsorbent's ability to regenerate suggests that treating industrial wastewater can be achieved easily and efficiently. The efficiency of the adsorption process was enhanced through optimization using the Box-Behnken Design (BBD).

1. Introduction

The possible toxicity of dyes to aquatic ecosystems and human health makes their presence in wastewater a major cause for worry (El-Desouky et al., 2022). These dyes, which frequently include aromatic chemicals and heavy metals, can disturb ecosystems, cause oxygen depletion in bodies of water, and bioaccumulate in living things, posing hazards further up the food chain. Furthermore, long-term toxicity issues are made worse by their continued presence in the environment (Mittal et al., 2007). To try to reduce the toxicity of this material, a range of treatment methods are utilized in conjunction with discharge control

requirements, such as chemical oxidation and biological treatment. By taking these steps, the harmful impacts of dye contamination will be reduced, protecting the environment and the general public's health.

Wastewater originating from different industrial processes frequently contains a wide range of colors, each with unique chemical characteristics and uses. Reactive dyes are frequently found in wastewater because of their water solubility and ability to establish strong interactions with fibers, which contribute to their bright hues when used in textiles (Fiorito et al., 2023). Direct dyes are frequently used to color natural textiles like cotton and wool because of their ease of use and adaptability (Gautam et al., 2015). Acid dyes are another common type

* Corresponding author at: Department of Chemistry, College of Science, University of Tabuk, Tabuk, Saudi Arabia.

E-mail address: nmmohamed@uqu.edu.sa (N.M. El-Metwaly).

<https://doi.org/10.1016/j.arabjc.2024.106035>

Received 29 April 2024; Accepted 23 October 2024

Available online 26 October 2024

1878-5352/© 2024 The Authors. Published by Elsevier B.V. on behalf of King Saud University. This is an open access article under the CC BY-NC-ND license (<http://creativecommons.org/licenses/by-nc-nd/4.0/>).

found in wastewater and are well-known for their capacity to color protein-based textiles like silk and wool. Because of their cationic qualities, basic dyes are frequently used to color synthetic textiles and are selected for their vivid shades. In order to color synthetic fibers like polyester and acetate, disperse dyes which are insoluble in water are necessary (Martini et al., 2018). The complex blend of hues found in wastewater is further enhanced by vat dyes, Sulphur dyes, and other specialist varieties, which represent the variety of industrial processes and ingredients (Fernández-Andrade et al., 2022).

Safranine, a dye used in biological staining and industrial applications, can be harmful to both people and the environment. For humans, exposure can cause respiratory issues if inhaled, stomach problems if ingested, and skin or eye irritation upon contact. Prolonged exposure can lead to allergic reactions (Mittal, 2020; Dhar et al., 2007). In the environment, safranine is particularly dangerous to aquatic life, disrupting ecosystems by reducing light for photosynthesis and potentially accumulating in the tissues of organisms, which can affect the entire food chain. It also poses risks to microorganisms, which are vital for wastewater treatment processes. To reduce these risks, safranine is often removed from water using adsorption techniques, where materials like activated carbon or metal-organic frameworks trap the dye molecules. This helps lower its concentration and minimize its harmful effects. Proper handling and disposal are essential to managing its toxicity (Mittal et al., 2010).

Diverse techniques are employed to extract dyes from wastewater, according to the wide variety of dye kinds and concentrations that are encountered. Adsorption technique are simple and versatile, but they require the replacement of adsorbents on a regular basis since they bind dye molecules to solid surfaces like activated carbon (Mahmoud et al., 2020). Though their effectiveness varies depending on the solubility of the dye, coagulation and flocculation processes destabilize dye molecules, allowing for their removal by sedimentation or filtration (Ouassif et al., 2020). The biological treatment method uses microorganisms to break down pigments in an environmentally beneficial way, however it takes longer to process the dyes. Although there may be financial and energy consequences, oxidation techniques, such as chemical and sophisticated oxidation procedures, convert dyes into non-toxic byproducts (George et al., 2023). Ion exchange uses resin exchange to selectively remove charged dyes, whereas membrane filtration physically separates dye molecules according to size and charge (Gaur et al., 2024; Rai et al., 2023). For some dye types, precipitation procedures work well because they create insoluble complexes with the dyes that require further separation (Mittal et al., 2006). For effective dye removal from wastewater, a combination of technique is frequently required, depending on factors including dye properties, cost, regulatory constraints, and environmental impact (Wan Ngah et al., 2010).

The process of adsorption is a very efficient and adaptable way to eliminate impurities from wastewater (Klett et al., 2014). Because of its versatility and ability to target a wide range of pollutants, including organic compounds, heavy metals, and dyes, it is a preferred alternative for wastewater treatment (Mittal et al., 2021; Patel et al., 2021; Mittal et al., 2021). The method is economical because it uses a lot of easily regenerated and widely available adsorbent materials, which lowers operating expenses (Mittal et al., 2021; Jain et al., 2014). Its capacity for selective elimination also makes it possible to treat particular pollutants keeping largely untouched other wastewater constituents (Naushad et al., 2016; Mariyam et al., 2021). With less sludge or byproduct production, this eco-friendly method fits very nicely with sustainability objectives. Adsorption provides a workable and effective solution for wastewater treatment and environmental remediation projects, making it an important instrument in the fight against water pollution (Zhang et al., 2020; Saharan et al., 2023).

Metal-organic frameworks (MOFs) have remarkable properties that make them very promising for the adsorption and elimination of dyes from wastewater (Kaushal et al., 2023). Due to MOFs' large surface area and adaptable pore structures, which allow them to effectively capture

dye molecules from water even at low concentrations, wastewater treatment processes can be made more effective. By adjusting the pore size and surface chemistry of MOFs at the molecular level, one can maximize their selectivity and adsorption capabilities for particular dye pollutants. Moreover, MOFs can be reused and recycled, reducing the overall cost and environmental impact of color removal processes (Soni et al., 2023; Dutta et al., 2022). Their broad applicability in a variety of industrial contexts is further enhanced by their diversity in composition and synthesis. By utilizing these special qualities, MOFs contribute significantly to the advancement of environmentally friendly wastewater treatment methods and the maintenance of ecosystem health and water quality (Ansari et al., 2011; Arora et al., 2021).

Box-Behnken Design (BBD) was chosen for optimization because it offers a practical and efficient approach to experimenting with multiple factors. One of the main benefits is that it requires fewer experiments compared to other designs, like Central Composite Design (CCD), making it more resource- and time-efficient. Additionally, BBD focuses on testing within a safer and more manageable range of conditions, avoiding extreme values that could be difficult or unsafe to work with. This design is also effective at capturing both linear and quadratic effects, helping researchers understand how different factors interact and influence the process. By using BBD, it's possible to find the best conditions for removing tartrazine dye while minimizing the number of experiments needed, making it a smart choice for optimization studies like this one (Ranjbari et al., 2022; Tabrizi et al., 2022).

For researchers and engineers, the BOX-Benken (BB) design technique offers a streamlined approach to optimizing the adsorption process, along with many benefits. Through the methodical variation of several elements at the same time, all while preserving orthogonality and balance, the BB design facilitates effective parameter space exploration in fewer experimental runs. Save time and money, and gain a comprehensive understanding of the factors influencing adsorption performance. BB design finds important factors and their interactions by statistical analysis technique like analysis of variance (ANOVA), which directs focused optimization efforts. Furthermore, by assessing a broad variety of operating conditions, the methodology improves the resilience and repeatability of optimization studies and helps identify the best parameter settings for maximum adsorption efficiency. In the end, BBD design promotes the creation of deeper understanding of adsorption mechanisms, decision-making instruments, and predictive models, ultimately leading to the design of effective adsorption systems for environmental remediation and wastewater treatment (Joshiba et al., 2022).

This investigation introduced a novel substance known as Tb-MOF, effectively eliminating the tartrazine dye E-102 (TZ) from water. The sponge possessed a substantial surface area and exhibited outstanding TZ adsorption properties. The investigation thoroughly examined the influence of various factors on the adsorption process, encompassing pH, contact time, TZ concentration, adsorbent dosage, and temperature. Statistical optimization applied the Box-Behnken experimental design technique was utilized to identify the most favorable adsorption conditions. In-depth characterization studies unveiled that the mechanism for TZ removal entailed an endothermic, chemisorptive process, with robust chemical interactions forming between trimethoprim and the functional groups on the sponge surface. Thermodynamic analyses substantiated the spontaneous nature of the adsorption process. Notably, the TB-MOF demonstrated high effectiveness as a potential adsorbent for purging TZ from polluted water sources. Overall, this investigation offers valuable insights into applying Tb-MOF materials in sustainable water treatment approaches for efficiently eliminating newly discovered pollutants.

2. Material and methods

2.1. Materials and instruments

The entire instrument description was thoroughly detailed in the



Fig. 1. Diagram showing the adsorption of TZ onto Tb-MOF.

Supplementary material (Tables S1 and S2) (Al-Hazmi et al., 2024).

2.2. Synthesis of Tb-MOF

There is a simple, eco-friendly method for producing Tb-MOF adsorbent. Equimolar amounts of methanol and Milli-Q water were mixed in a 100 mL container together with 4.48 g (0.012 mol) of Tb (Cl)₃·6H₂O and 4.05 g (0.05 mol) of 2-methyl imidazole (Hmim). A centrifuge was used to separate the white powdered product from the solution following a day of shaking the combination at room temperature (Gamoudi and Srasra, 2019). To eliminate any last organic linkers from the micropores, the powder was washed, filtered, and then cooked in methanol for an overnight period. The final Tb-MOF product's morphological features and structure are displayed in Fig. 1.

2.3. Removal and batch studies of the Tb-MOF

The optimal adsorption parameters for the color tartrazine (TZ) were evaluated using a 1000 ppm stock solution. Afterwards, working solution concentrations varied between 2.76×10^{-4} to 2.3×10^{-3} mmol/L were created using the stock solution. For all the solutions, deionized water was used. The effectiveness of Tb-MOF in removing the TZ dye was investigated by multiple batch adsorption experiments. Following the addition of the required quantity of Tb-MOF adsorbent to solutions with a constant dye concentration, the mixture was stirred vigorously. Samples were taken out and centrifuged at 6000 rpm at pre-arranged intervals after the concentration of the dye used in UV-vis spectroscopy (at 426 nm as maximum wavelength) (Nassef et al., 2024; El-Fattah et al., 2024; Alsuhaibani et al., 2024). To make an industrial sample of 25 ml, four samples from different locations were mixed with distilled water. This sample was used to evaluate the effectiveness of Tb-MOF in wastewater treatment. Following that, 0.02 g of Tb-MOF adsorbent was added to this sample and agitated for 100 min at pH 4, 298 K to test if any pollutants could be removed (Eq. S1 and S2) (Al-Hazmi et al., 2022).

2.4. Experimental design

The Response Surface Methodology is a helpful technique for conducting experiments to determine the best combinations of various components to produce the desired response (RSM). In this procedure, one particular set of technique used is the Box-Behnken design (BBD). By applying mathematical models to three-level incomplete factorial de-

signs, BBD accounts for first- and second-order coefficients (Al-Hazmi et al., 2024). Assume the following four independent variables: temperature, pH, time, and pH. Create an example scenario where the goal is to maximize the adsorption capacity. According to Eq. (1), this led to the conduct of three separate test levels: negative one, zero, and positive one (Table S3). Ultimately, RSM allows us to understand how to design the best possible solution for our situation, which ultimately allows us to actualize great outcomes (Almahri et al., 2023).

$$Y = \beta_0 + \sum \beta_i X_i + \beta_{ii} X_i^2 + \sum \sum \beta_{ij} X_i X_j \quad (1)$$

3. Results and discussion

3.1. Characterization of Tb-MOF

3.1.1. Patterns of X-ray diffraction (XRD)

Hmim anions' interactions with Tb ions on the surface raised the crystallinity level of the Tb-MOF. To calculate the crystal structure of the MOF system with Tb, computations were carried out using the software program Foolproof and Check Cell. The outcome showed the presence of an orthorhombic crystal structure in the P222 space group. The calculated parameters provided information on the crystal dimensions: $a = 22.58 \text{ \AA}$, $b = 18.92 \text{ \AA}$, $c = 5.81 \text{ \AA}$, $\alpha = 90^\circ$, $\beta = 90^\circ$, $\gamma = 90^\circ$. Surprisingly, even after adsorption, the Tb-MOF nanospheres kept their diffraction peaks. This demonstrates the crystal structure's exceptional endurance (Fig. 2(a)) (Al-Hazmi et al., 2024; Al-Hazmi et al., 2024; Alaysuy et al., 2024).

3.1.2. N₂ adsorption/desorption

Mesoporous materials can be identified by their type II N₂ adsorption/desorption isotherms. A Type II nitrogen (N₂) adsorption/desorption isotherm describes gas adsorption on non-porous or macroporous solids, where multilayer adsorption occurs. At low pressures (P/P_0), adsorption begins with a monolayer and transitions into multilayer adsorption, marked by an inflection point used to estimate surface area via BET theory. As pressure rises, adsorption increases steadily, forming a convex curve until it levels off near $P/P_0 = 1$, indicating surface saturation. Desorption is generally reversible, with possible slight hysteresis. Type II isotherms are key for analyzing surface area and multilayer adsorption behavior (Mogharbel et al., 2024; Alsuhaibani et al., 2023; Alsharief et al., 2024). The combination of these characteristics creates a hysteresis loop between the desorption and adsorption

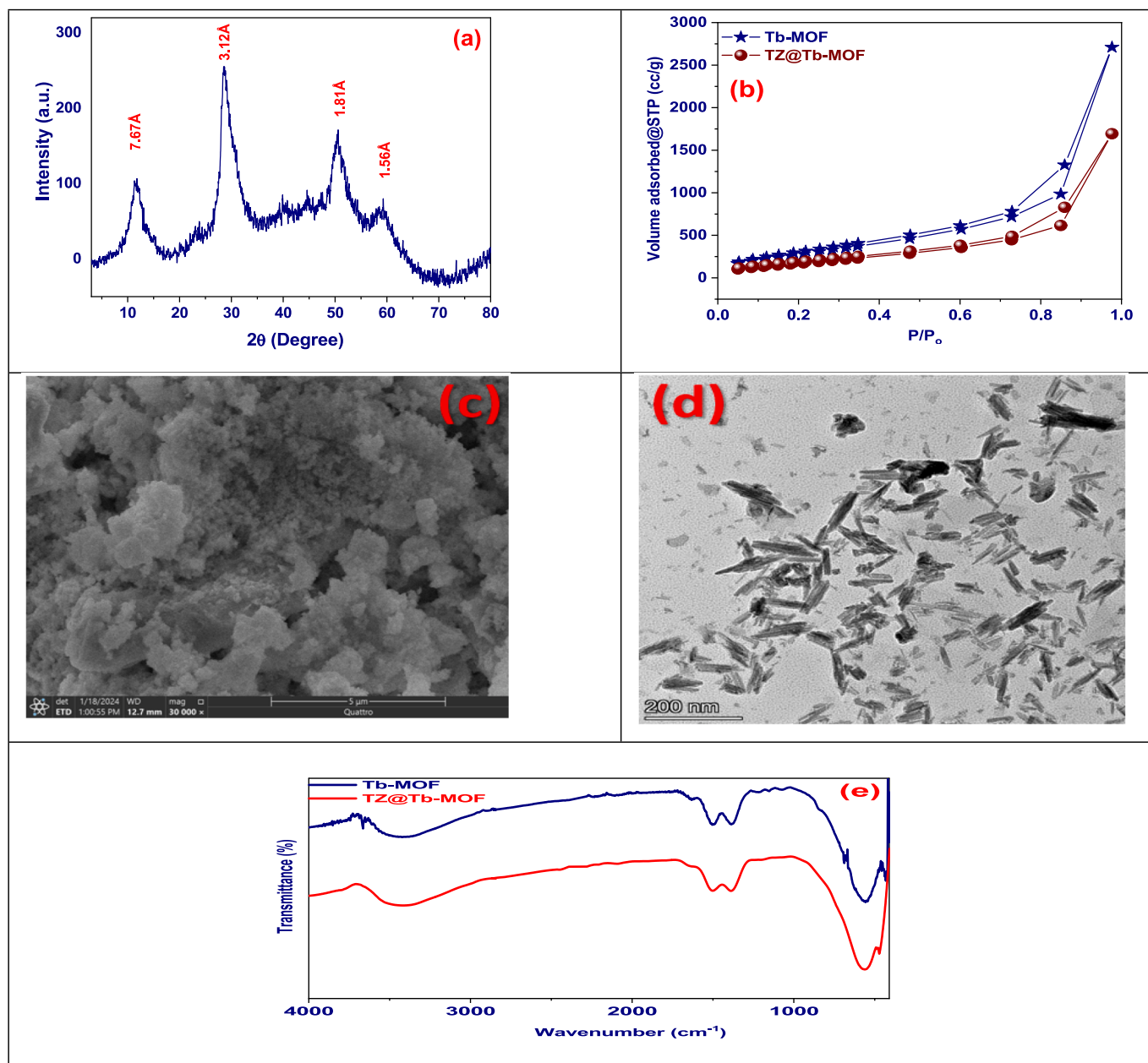


Fig. 2. (a) XRD pattern of Tb-MOF, (b) N_2 adsorption/desorption of Tb-MOF and TZ@Tb-MOF, (c) SEM image, (d) TEM image, and (e) FT-IR of Tb-MOF and TZ@Tb-MOF.

branches, highlighting the fact that gas molecules are not leaving in the same order as they arrived. The H3 hysteresis loop is seen in adsorption/desorption isotherms of materials with slit-shaped mesopores, such as plate-like particles. It arises from differences between adsorption, where gas condenses in pores, and desorption, where gas evaporates at lower pressures, creating a pronounced loop. The absence of a plateau at high pressures indicates incomplete pore saturation, and the steep desorption branch reflects the abrupt gas release from wide or slit-shaped pores, typical of materials like clays or layered structures. This hysteresis suggests a subtle dynamic that is important to comprehend the mesoporous material's complex size distribution, accessibility, and pore structure. Thus, the Type II isotherm unlocks possibilities in areas such as gas storage and catalysis by acting as a guide for researchers exploring the world of mesoporous materials. With a specific surface area of $1123.07 \text{ m}^2 \cdot \text{g}^{-1}$, pore volume 4.02 cc/g , and pores size 7.8 nm . Which after adsorption were decreased to $762.8 \text{ m}^2 \cdot \text{g}^{-1}$, 2.6 cc/g , and 3.2 nm , respectively. This adsorbent may be categorized as a mesoporous

material by the "IUPAC". The surface area, pore volume, and size decreased following TZ dye adsorption, suggesting that some of the adsorption mechanism occurred through the adsorbent's pores (Fig. 2 (b)).

3.1.3. SEM and TEM analysis

The SEM (Scanning Electron Microscopy) images of Tb-MOF, which display rod-like structures, that confirmed by analysis with TEM have helped to clarify the morphological characteristics of this Terbium Metal-Organic Framework. The rods' appearance indicates a certain arrangement of long-term particles or crystals within the MOF. This morphology increases the surface area, providing more active sites for adsorption and improving pore accessibility, allowing better diffusion of guest molecules into the framework. Additionally, the rod-like shape contributes to the structural stability of the MOF, ensuring it maintains integrity during adsorption/desorption cycles. This structure also supports a more uniform pore-filling mechanism, benefiting selective

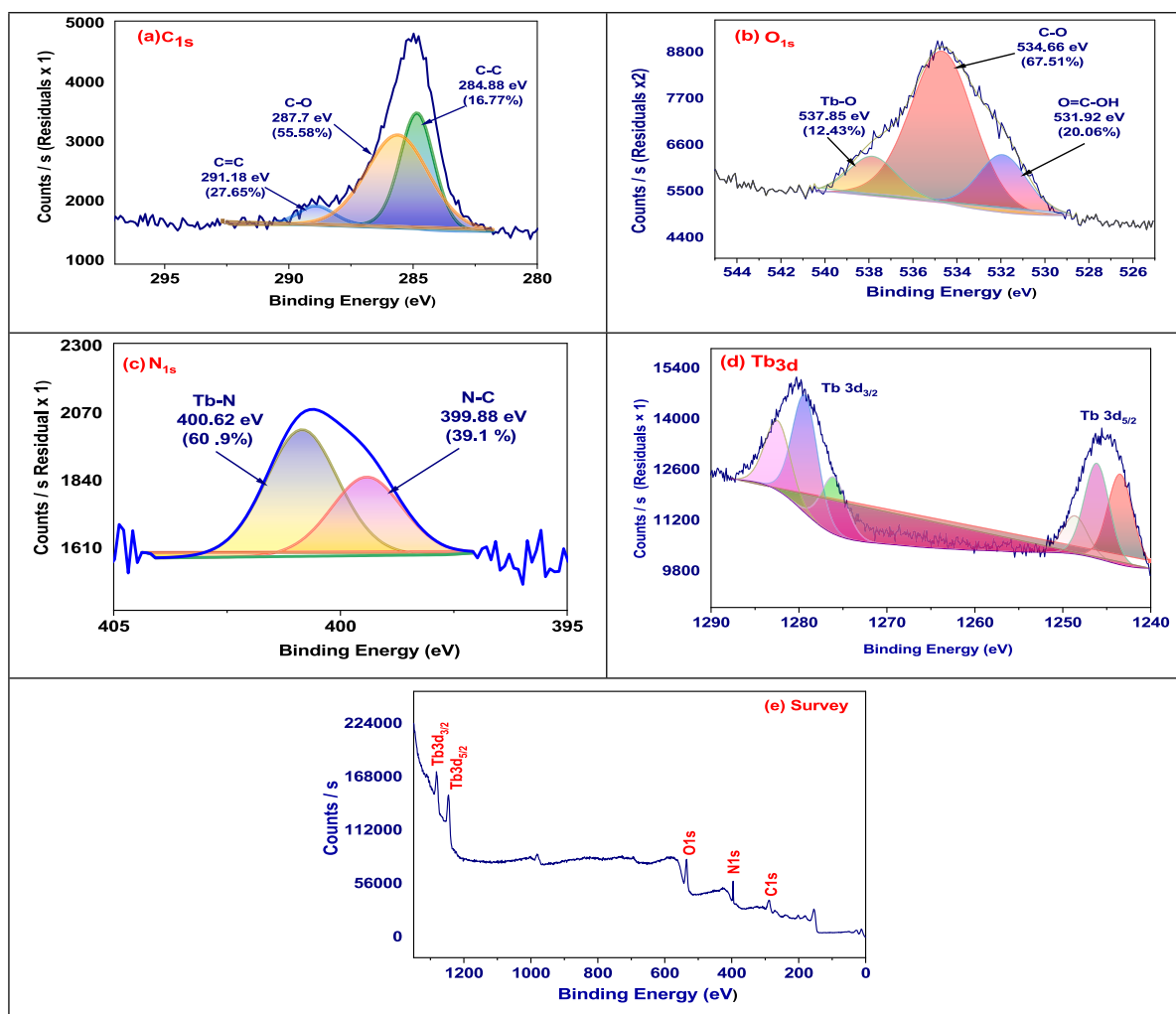


Fig. 3. XPS of Tb-MOF.

adsorption through electrostatic interactions and size-exclusion effects. There, experts will most likely provide in-depth explanations for the observed morphology in addition to discussing its significance in relation to the synthesis, traits, and potential applications of Tb-MOF (Fig. 2(c)). These porous structures demonstrate the possibility of synthesizing Tb-MOF, which makes it appropriate for the adsorption of dyes. Tb-MOF microspheres are studied using TEM. The morphology of this Tb-MOF is seen in Fig. 2(d). It is possible to see the length of the adsorbent, which is between 30 and 50 nm. Transmission electron microscopy (TEM) photos show that the Tb-MOF with good dispensability, and the composite particles have a spherical form (Almahri et al., 2023; Alrefaee et al., 2023; Al-Qahtani et al., 2023).

3.1.4. FT-IR

The Fourier-transformed infrared (FTIR) spectra of the synthesized Tb-MOF were depicted in Fig. 2(e), both before and after the removal of TZ. The broad band at 3439 cm^{-1} might be the result of water molecules' O-H stretching vibration after they have been adsorbed to a substance's surface. Accordingly, the asymmetric stretching vibrations of the aromatic and aliphatic C-H were linked to the peaks at 2978 cm^{-1} . In contrast, the C=N stretch vibration was suggested by the band at 1503 cm^{-1} . The complete ring stretching was characterised by the bands at 1482 and 1389 cm^{-1} . Consequently, the maxima at 1084 and 790 cm^{-1} can be connected to the C-N bending vibration and the C-H bending mode (Almahri et al., 2023; Alluhaybi et al., 2023; Aljohani et al., 2023). The Tb-N vibration at 695 cm^{-1} produced the band.

Furthermore, in the setting of Tb-MOF, the link between 2-methyl imidazole and the metal centre is revealed by the absence of the peak at 1843 cm^{-1} of the -NH stretching frequency created by 2-methyl imidazole.

3.1.5. XPS

The chemical composition of Tb-MOF may be thoroughly understood thanks to XPS analysis. For high-resolution scans, we can statistically examine the signals' integral intensity or peak area (Almahri and El-Metwaly, 2024). Gaining insight from this understanding will enable us to better understand these compounds (Fig. 3).

3.2. Batch experiments

3.2.1. Effect of point of zero discharge

The neutral charge point (pH_{PZC}) was determined using a solid addition method (Mariyam et al., 2021). A set of 0.1 M KNO_3 solutions (50 mL each) were prepared and their pH levels were adjusted within the range of 2.0 to 12.0 by adding 0.1 or 0.01 mol/L of HCl, and 0.1 or 0.01 mol/L of NaOH. 0.1 g of Tb-MOF was added to each solution and the mixtures were manually shaken. The solutions were then kept at 293 K for 48 h with occasional manual agitation. The final pH of the solutions was recorded and the difference was graphed against the initial pH (X-axis) and the change in pH (ΔpH) (Y-axis) (Hassan et al., 2020). The relationship between pH and dye removal can be demonstrated using the adsorbent surface's isoelectric point. The dye adsorption process is

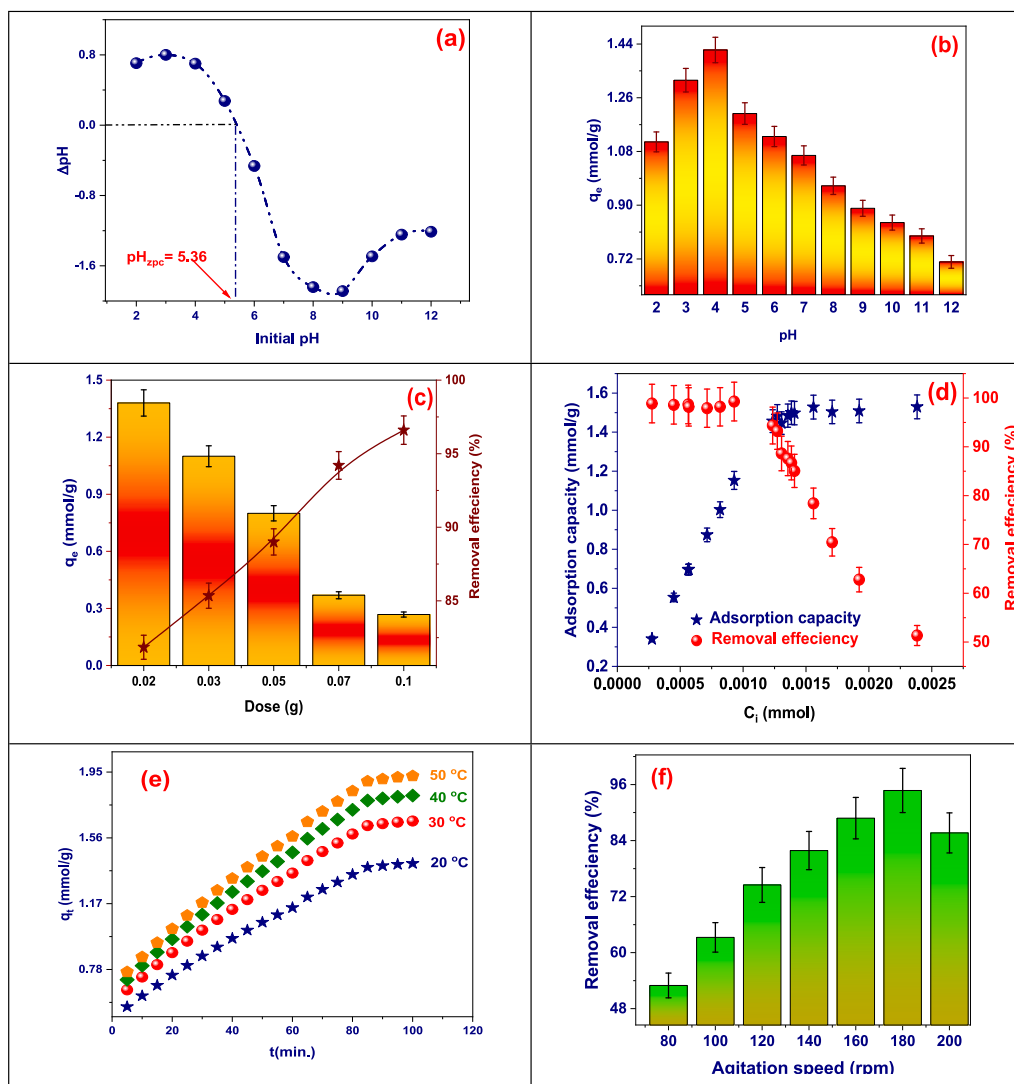


Fig. 4. (a) Determination of pH of point of discharge pH_{zpc} , (b) Effect of pH on adsorption of TZ (C_i : 1.356×10^{-3} mmol, time: 30 min., dose: 0.02 g, volume: 25 mL, agitation speed 180 rpm, and temp.: 25 °C), (c) Effect of dose (C_i : 1.356×10^{-3} mmol, time: 30 min., dose: 0.02 to 0.25 g, volume: 25 mL, agitation speed 180 rpm, and temp.: 25 °C), (d) Effect of initial concentration (C_i : 2.76×10^{-4} to 2.36×10^{-3} mmol, time: 100 min., dose: 0.02 to 0.25 g, volume: 25 mL, agitation speed 180 rpm, and temp.: 25 °C), (e) Effect of time and temperature (C_i : 1.556×10^{-3} mmol, time: 5 to 100 min., dose: 0.02 g, volume: 25 mL, agitation speed 180 rpm, and temp.: 20 to 50 °C), and (f) Effect of agitation speed on adsorption of TZ via Tb-MOF (C_i : 1.356×10^{-3} mmol, time: 30 min., dose: 0.02 g, volume: 25 mL, agitation speed 80 to 200 rpm, and temp.: 25 °C).

significantly impacted by the pH level of the solution. In addition, it alters the adsorbent's surface charge, the structure of the dye molecules, and the extent to which various contaminants ionize. At pH_{PZC} , basic and acidic functional groups have no more effect on a liquid's pH. The pH_{PZC} (zero-point charge) of Tb-MOF was found to be 5.36 (Al-Hazmi et al., 2023; El-Metwaly et al., 2022). The positively charged sorbent surface has the ability to draw anions out of the solution when the pH of the mixture is lower than pH_{PZC} . Because Tb-MOF has a negatively charged surface, it draws cations when the pH of the solution is higher than pH_{PZC} . Here, a lower pH is preferable for the removal of dye because it creates more positively charged sites, which make it easier for negatively charged dye ions to bind to them through the electrostatic force of attraction (Fig. 4 (a)).

3.2.2. Effect of pH

The pH range of 2 to 12 was used to study the solution's pH effect. From pH = 2 to pH = 4, the efficiency of the dye retention by Tb-MOF improves from 1.11 to 1.42 mmol/g, as shown in Fig. 4(b) (El-Desouky et al., 2022; El-Desouky et al., 2022). The retention steadily drops at pH

values greater than 5.36, reaching 0.7 mmol/g at pH = 12. While the partial dissolving of the adsorbent in an acidic environment is responsible for the decrease in retention, the competition with OH^- ions for adsorption sites in a basic medium may also play a role. The relationship between pH and dye adsorption can be demonstrated using the point of zero charge value (PZC). The pH at which the adsorbent's charge value is zero is known as the PZC. The adsorbent surface charge balance may employ the PZC as a parameter. The PZC of Tb-MOF is 5.38 (Fig. 4(a)).

The adsorption of dyes like tartrazine depends on the interaction between the dye's chemical properties and the surface of the adsorbent, both of which are influenced by pH. Tartrazine has three key pKa values 2, 5, and 10.86 meaning its form changes with pH. Below pH 2, it is neutral, while above pH 2, it starts to lose protons and becomes anionic, fully deprotonating after pH 10.86. These changes affect how it interacts with the adsorbent. The adsorbent's charge, determined by its point of zero charge (PZC) was 5.36, also varies with pH. When the pH is below the PZC, the surface becomes positively charged, favoring attraction to the negatively charged dye so, the optimum pH for adsorption and removal of TZ was at pH 4. Above the PZC, the surface turns negatively

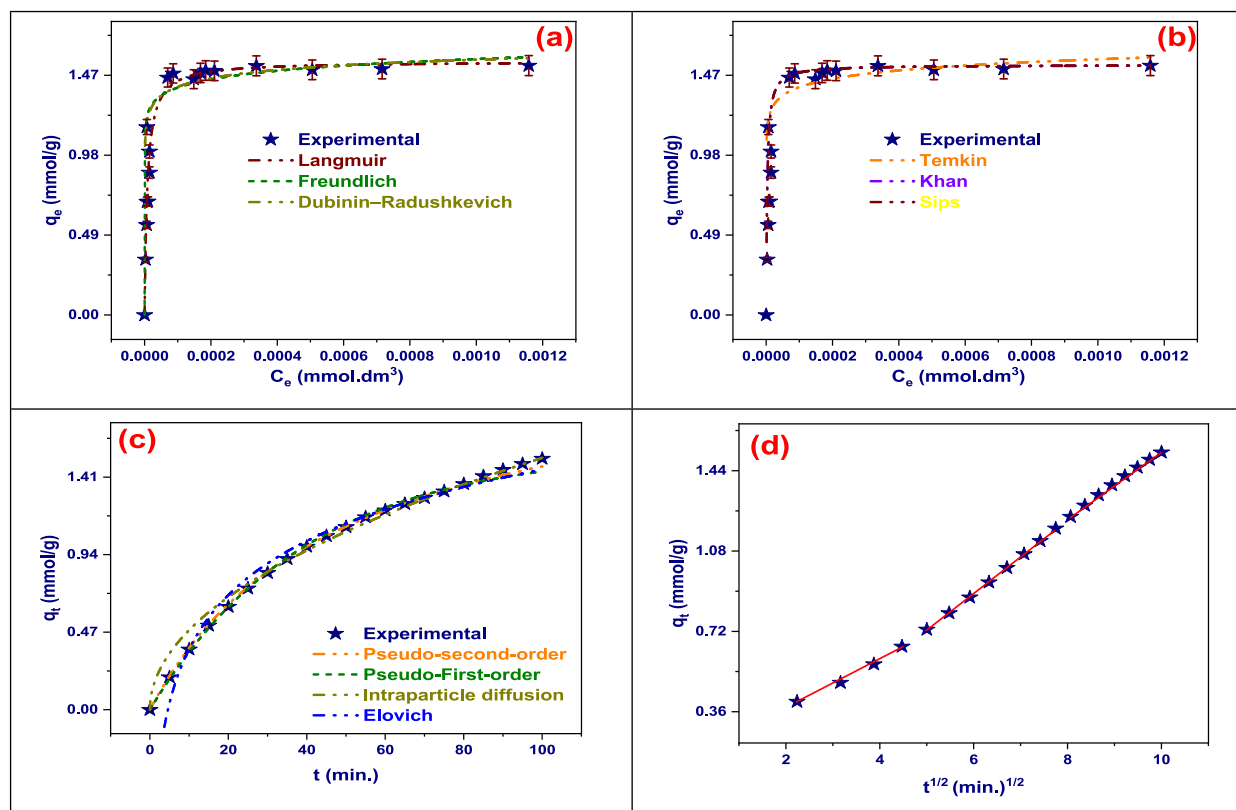


Fig. 5. (a and b) Adsorption isotherm model (C_i : 2.76×10^{-4} to 2.36×10^{-3} mmol, time: 100 min., dose: 0.02 to 0.25 g, volume: 25 mL, agitation speed 180 rpm, and temp.: 25 °C), (c) adsorption kinetic model (C_i : 1.556×10^{-3} mmol, time: 5 to 100 min., dose: 0.02 g, volume: 25 mL, agitation speed 180 rpm, and temp.: 25 °C), and (d) IPD for adsorption TZ onto Tb-MOF (C_i : 1.556×10^{-3} mmol, time: 5 to 100 min., dose: 0.02 g, volume: 25 mL, agitation speed 180 rpm, and temp.: 25 °C).

charged, which can reduce adsorption due to repulsion. In short, the balance between the pH, the dye's form, and the adsorbent's surface charge plays a crucial role in how well tartrazine is adsorbed.

3.2.3. Effect of dose

In Fig. 4(c), as the Tb-MOF dose is increased from 0.02 to 0.25 g for 25 mL of the TZ dye, the tartrazine removal efficiency was increased (Eq. S2). At 0.02 g, the adsorption capacity reached its optimum. The adsorption processes were affected by the active sites at the higher adsorbent dosage. From Eq. S1 it could postulated that the adoption capacity was inversely proportional to the adsorption capacity as the dose increase the adsorption capacity decrease. The concentration gradient plays a major role in determining the optimal adsorbent level for the adsorption process.

3.2.4. Effect of TZ dye concentration

As demonstrated in Fig. 4(d), the amount of TZ that was adsorption capacity increased from 0.34 to 1.53 mmol/g, while, the removal efficiency of TZ was decreased from 98.9 to 51.33 percent. According to the Eq. S2 as the initial concentration was inversely proportional to the removal efficiency, and on other hand, the adsorption capacity was increase as the initial concentration increase as well as the difference between initial and final concentration increase as it directly proportional to adsorption capacity (Alsharief et al., 2024).

3.2.5. Effect of contact time and temperature

The duration of contact is a highly important factor that needs to be finely tuned during the process, as it has a substantial impact on the removal efficiency of the adsorption process. The adsorption process was modified across a range of contact times (5 to 100 min) at various temperatures (20 to 50 °C) with a dosage of 0.02 g/25 mL in order to ascertain the optimal contact time. Fig. 4(e) illustrates the data on

equilibrium time for TZ adsorption. As the temperature increased, an increase in adsorption capacity was observed with increase the contact time and specially with increase the temperature (Alsuhaibani et al., 2023).

3.2.6. Effect of agitation speed

Fig. 4(f) shows that when equilibrium circumstances were established, the influence of agitation speed was found to be between 80 and 200 rpm. It demonstrates that the Tb-MOF reached its maximum adsorption at 180 rpm and had a total removal efficacy of 94.74 percent. Following an initial rise, removal efficiency began to decrease with increasing sample speeds. These findings suggest that the agitation speed significantly impacted the adsorption. Increased agitation may also be the source of this, as it results in greater turbulence and a thinner boundary layer around the sorbent particles (El-Desouky et al., 2022; Abd El-Wahab and El-Desouky, 2022; El-Desouky et al., 2022).

3.3. Adsorption isotherm

Every adsorption isotherm model has unique benefits for comprehending the interactions between adsorbate and adsorbent as well as insightful information about the adsorption process. For determining the maximal adsorption capacity and affinity, the Langmuir isotherm is especially helpful because it makes the assumption that monolayer adsorption occurs on a homogenous surface (Langmuir, 1916). However, the Freundlich model can be applied to a variety of concentrations and non-ideal adsorption conditions due to its versatility in defining multilayer adsorption on heterogeneous surfaces (Freundlich, 1906). Specifically created to examine adsorption onto microporous materials, the Dubinin–Radushkevich model provides insight into the energetics of adsorption (Dubinin, 1947). Temkin isotherms are useful for systems with heterogeneous surfaces because they explain the non-uniform

distribution of heat of adsorption and the interactions between the adsorbate and the adsorbent. The Khan model improves the accuracy of the Langmuir isotherm in some situations by extending it to take into account lateral interactions between adsorbate molecules (Tempkin, 1940). Last but not least, the Sips isotherm provides versatility in characterizing adsorption behavior from monolayer to multilayer coverage by combining elements of the Freundlich and Langmuir models. The optimization of adsorption processes for wastewater treatment and environmental remediation is made possible by the combined contribution of these models to a thorough understanding of adsorption phenomena (Table S4).

TZ's adsorption onto Tb-MOF can be demonstrated using the Langmuir adsorption isotherm model, which provides a systematic approach to measuring the adsorption process and understanding its fundamental concepts. Fitting experimental data to the Langmuir equation yields important properties such as the equilibrium constant and maximum adsorption capacity. This enables the interaction between TZ molecules and the Tb-MOF surface to be understood quantitatively by researchers. Furthermore, the Langmuir model's assumption of monolayer adsorption on a homogenous surface may allow for a more standardized and straightforward method of characterizing the adsorption behavior (Langmuir, 1916). This enables predictive modelling of the process under different conditions and facilitates comparison of the adsorption process with other adsorbent materials Table S5. In the end, the Langmuir model helps us better understand the effectiveness of Tb-MOF for wastewater dye removal and its possible uses. This helps us design effective adsorption systems for environmental remediation (Fig. 5(a, b)).

The Freundlich adsorption isotherm model is a versatile and useful tool for describing TZ's adsorption onto Tb-MOF. The versatility of this model in characterizing heterogeneous surfaces and allowing for multilayer adsorption makes it an excellent choice for explaining the intricate interactions that occur between TZ molecules and the Tb-MOF surface. Through the calculation of Freundlich model parameters, including the Freundlich constant (K_F was 2.2 (mmol/g)(L/mmol)^{1/n}) and exponent (1/n was 0.056), Researchers are able to measure the favorability and extent of adsorption quantitatively, which gives them important information about how adsorption works (Freundlich, 1906). A thorough grasp of the adsorption process is also made possible by contrasting the characteristics of the Freundlich model with those derived from other models, such as the Langmuir model. By determining whether adsorption happens primarily through monolayer or multilayer coverage, this comparative investigation helps to clarify the underlying mechanisms of adsorption onto Tb-MOF. All things considered, using the Freundlich model improves our comprehension of TZ's adsorption behavior onto Tb-MOF and makes it easier to optimize adsorption procedures for effective dye removal from wastewater (Table S6).

The adsorption of TZ onto Tb-MOF is demonstrated using the Dubinin–Radushkevich (D-R) adsorption isotherm model, which offers a comprehensive way to understand the adsorption mechanism and energy aspects of the process. The D-R model provides insights into the specific surface characteristics and pore structure of Tb-MOF. It is designed for the analysis of adsorption onto microporous materials. By estimating parameters such as the mean free energy of adsorption and the limiting adsorption capacity, the D-R model yields quantitative information about the strength of interactions between TZ molecules and the Tb-MOF surface, as well as the maximum adsorption capacity under specific conditions (Dubinin, 1947). This makes it possible to comprehend the adsorption process more thoroughly, especially in regards to deviations from ideal monolayer adsorption and non-ideal adsorption behavior. Additionally, contrasting the parameters of the D-R model with those of other models provides important information on the surface characteristics and dominating adsorption mechanism of Tb-MOF, which helps optimize adsorption procedures for effective dye removal from wastewater. The most likely adsorption process was chemisorption, as shown by the adsorption energy of 23.78 kJ/mol.

The adsorption of TZ onto Tb-MOF can be illustrated using the Temkin adsorption isotherm model, which provides a thorough understanding of the energetics and interactions involved in the process. This model sheds light on the intricate nature of adsorption onto heterogeneous surfaces like Tb-MOF by accounting for the non-uniform distribution of heat of adsorption and adsorbate-adsorbent interactions. The Temkin model helps characterize the adsorption mechanism by providing quantitative information about the average energy of adsorption per mole of adsorbate by estimating parameters like the adsorption heat (B). Furthermore, its robustness in less-than-ideal systems makes it possible to analyze adsorption behavior with confidence, especially when interactions or surface characteristics differ from ideal circumstances. Understanding is further improved by comparison study with various adsorption isotherm models, which clarifies the predominant adsorption mechanism onto Tb-MOF. In general, the utilization of the Temkin model enhances our understanding of the TZ adsorption process onto Tb-MOF, hence aiding in the optimization of adsorption systems for effective wastewater dye removal (El-Desouky et al., 2022; El-Bindary et al., 2022).

A thorough understanding of the energetics and interactions involved in the process can be gained by using the Temkin adsorption isotherm model to illustrate the adsorption of TZ onto Tb-MOF. This model sheds light on the intricate nature of adsorption onto heterogeneous surfaces like Tb-MOF by accounting for the non-uniform distribution of heat of adsorption and adsorbate-adsorbent interactions. The Temkin model provides quantitative information on the average energy of adsorption per mole of adsorbate by estimating factors like the adsorption heat, which helps characterize the adsorption mechanism. Additionally, because of its resilience in less-than-perfect systems, a trustworthy analysis of adsorption behavior is possible, especially when interactions or surface characteristics differ from ideal circumstances. By clarifying the predominant adsorption mechanism onto Tb-MOF, comparative comparison with other adsorption isotherm models further advances comprehension. In general, the Temkin model's use deepens our understanding of the TZ adsorption process onto Tb-MOF and aids in the development of adsorption systems that are optimal for the effective removal of dye from wastewater.

An effective way to comprehend the intricate interactions taking place at the adsorbent surface is to use the Khan adsorption isotherm model to show how TZ is adsorbed onto Tb-MOF. The Khan model provides better adsorption behavior description by expanding the Langmuir isotherm to include lateral interactions between adsorbate molecules, especially in situations where cooperative or competitive interactions are important. This improved precision makes it possible to characterize the adsorption mechanism onto Tb-MOF more precisely, which advances our understanding of the procedure. Moreover, the Khan model's predictive powers enable the calculation of critical adsorption parameters, which support the design of efficient dye removal systems and the optimization of adsorption processes. Further insights into the primary adsorption mechanism and the impact of lateral interactions on adsorption behavior can be gained by comparative analysis with other adsorption models. All things considered, the use of the Khan adsorption isotherm model advances our knowledge of the TZ adsorption process onto Tb-MOF and directs the creation of effective adsorption systems for the treatment of wastewater (Tempkin, 1940).

A thorough and adaptable method for analyzing the adsorption of TZ onto Tb-MOF is to use the Sips adsorption isotherm model. The Sips model describes adsorption events from monolayer to multilayer coverage with versatility by combining elements from both Langmuir and Freundlich isotherms. Understanding the intricate adsorption behavior onto Tb-MOF, where numerous interactions and coverage levels may be involved, is made easier with this flexibility. Furthermore, our comprehension of the underlying mechanisms involved in the process is boosted by the increased precision of the Sips model. It supports dye removal system optimization by enabling the measurement of

critical adsorption parameters through parameter estimation.

3.4. Adsorption kinetics

A variety of adsorption kinetic models, including the Elovich (Weber and Morris, 1963), pseudo-first-order (Lagergren, 1898), pseudo-second-order (Ho and McKay, 1998), and intraparticle diffusion models, can be used to obtain a thorough understanding of the kinetics of adsorption processes. A thorough examination of adsorption kinetics is made possible by the distinct insights that each model offers into various facets of the adsorption process. Important parameters like equilibrium adsorption capacities and rate constants can be found by fitting experimental data to these models, yielding quantitative insights into the adsorption process. Furthermore, these models are predictive in nature, making it possible to estimate the behavior of adsorption under different situations and to optimize adsorption procedures for wastewater treatment applications (Table S4). By assessing the effectiveness and applicability of several kinetic models for characterizing adsorption kinetics, comparative examination of these models contributes to our understanding by highlighting the main mechanisms governing adsorption. All things considered, the application of adsorption kinetic models advances our knowledge of adsorption mechanisms and facilitates the development of effective adsorption systems for environmental remediation (Fig. 5(c)).

The adsorption of TZ onto Tb-MOF can be studied using the Pseudo-First-order kinetic model, which provides a simple and effective way to conduct preliminary investigation. The ease of use of this model facilitates rapid parameter estimate, which offers significant insights into the capacity and rate of adsorption onto Tb-MOF (Lagergren, 1898). It provides a valuable method for comprehending early-stage adsorption behavior and is especially helpful in explaining the first adsorption stage, when TZ concentrations are high. Researchers can evaluate the model's applicability and suitability for accurately explaining the adsorption kinetics by comparing it with experimental data through comparative analysis. Its simplicity of use also makes it possible to quickly evaluate and screen adsorption processes, which directs additional research and optimization efforts. For this reason, the Pseudo-First-order kinetic model is a useful tool for understanding the adsorption kinetics of TZ onto Tb-MOF and for optimizing adsorption procedures in wastewater treatment applications (Table S5).

The pseudo-second-order kinetic model is a dependable and accurate way for comprehending the adsorption kinetics of TZ onto Tb-MOF. This model provides a more realistic representation of the adsorption process than the pseudo-first-order model since it considers chemisorption to be the rate-limiting step (Ho and McKay, 1998). The equilibrium adsorption capacity (q_e) and the rate constant (K_2) that are derived from the pseudo-second-order model provide important information on the maximum adsorption capacity and adsorption rate onto Tb-MOF. Optimizing processes is also made easier by the mechanistic insights this model offers, which improve our comprehension of the fundamental mechanisms controlling the adsorption behavior. The Pseudo-second-order model's predictive powers allow for the calculation of adsorption behavior under various circumstances, which directs the design and optimization of adsorption systems for effective dye removal from wastewater. The correctness and appropriateness of the model for accurately characterizing the adsorption kinetics are further validated by a comparative study with experimental data. All things considered, the utilization of the pseudo-second-order kinetic model contributes to our understanding of TZ adsorption onto Tb-MOF and makes the development of effective adsorption processes for wastewater treatment easier (El-Desouky et al., 2022; Al-Wasidi et al., 2022; Kiwaan et al., 2021).

The adsorption of TZ onto Tb-MOF may be studied using the Intraparticle diffusion kinetic model, which offers important insights into the diffusion mechanisms controlling the process. This model makes a clear distinction between intraparticle diffusion-controlled phases and

external surface adsorption, enabling a comprehensive understanding of mass transfer constraints within the adsorbent particle (Weber and Morris, 1963). The model provides quantifiable parameters, such as the diffusion rate constant and the intercept, providing information about the diffusion process within Tb-MOF. These parameters are obtained by evaluating the linear portion of the adsorption curve versus the square root of time. Additionally, it helps validate the adsorbent material's pore structure, offering vital details regarding how well it facilitates adsorption. Validating diffusion-controlled adsorption processes onto Tb-MOF through comparison of experimental data with the Intraparticle diffusion model ensures confidence in the model's accuracy. The utilization of the Intraparticle diffusion model, in general, improves our comprehension of the diffusion mechanisms that underlie TZ adsorption onto Tb-MOF and aids in the streamlining of adsorption procedures for the treatment of wastewater (Table S7).

Applying the Temkin kinetic model to the adsorption of TZ onto Tb-MOF allows for a comprehensive understanding of the underlying adsorption mechanisms. By accounting for interactions between the molecules of the adsorbate and the heterogeneous surface of Tb-MOF, the Temkin model provides insights into the energetics of the adsorption process. Its parameters help characterize the adsorption behavior by providing important information about the heat of adsorption and the strength of the adsorbate-adsorbent interactions. Furthermore, the Temkin model's predictive powers enable the assessment of adsorption behavior under various circumstances, which facilitates the design and improvement of adsorption systems for the treatment of wastewater. The correctness and appropriateness of the model may be evaluated by comparing it with experimental data, which improves our comprehension of the main adsorption mechanisms onto Tb-MOF. In general, the Temkin kinetic model is applied to improve our understanding of TZ adsorption onto Tb-MOF, which assists in the creation of effective adsorption procedures for the treatment of wastewater (Temkin, 1940).

3.5. Diffusion mechanism

To move from the solution to the adsorbent (solid) surface, the adsorbate must theoretically go through three main processes:

- (i) TZ molecules are initially moved from the main solution to the Tb-MOF surface externally (via film diffusion);
- (ii) Second, TZ molecules diffuse through Tb-MOF pores and arrive at the adsorptive regions (intraparticle diffusion);
- (iii) When TZ molecules are evenly spaced throughout the Tb-MOF surface, they create a strong bond with the positively charged substance.

The rate-limiting phases in the TZ adsorption process were investigated using the IPD model. The adsorption mechanism on a porous adsorbent consists of multiple processes. First, mass transfer through the external liquid film of the adsorbent; then, movement of the adsorbate molecule into the intraparticle (Alrefaee et al., 2023). The final stage involves adsorption onto the adsorbent's exterior or interior surfaces by chemical or physical bonding. Assuming a brief process for the last stage, the adsorption rate should be most affected by film or intraparticle diffusion. Plotting qt vs. $t^{0.5}$ aided in bettering the IPD by illuminating the adsorption process' mechanism. IPD is the sole adsorption control method if the line in the figure has a mathematical value of zero, passing through the origin. But, if the adsorption process manages to evade the source, additional mechanisms, such as liquid film diffusion, may be employed to control the process. The multi-linear plots of q_t vs. $t^{0.5}$ in Fig. 5(d) primarily displayed the behavior of three linear zones (Al-Qahtani et al., 2023). It demonstrates that intraparticle diffusion did not appear to be the rate-limiting phase during the whole adsorption process. The higher rate constants in the first stage could be attributed to the outer film diffusion of the Tb-MOF adsorbent; the equilibrium phase is

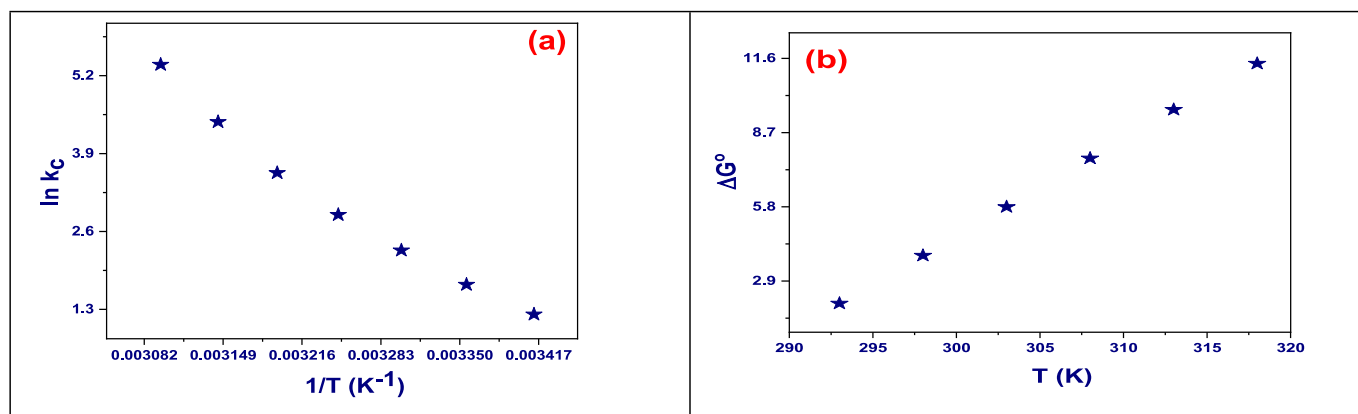


Fig. 6. Effect of temperature on adsorption TZ dye on Tb-MOF: (a) Van't Hoff, and (b) Effect of temperature on ΔG° (C_i : 1.556×10^{-3} mmol, time: 5 to 100 min., dose: 0.02 g, volume: 25 mL, agitation speed 180 rpm, and temp.: 20 to 50 °C).

followed by progressive intraparticle diffusion (this was established by the negative standards of X in the first stage). The rates of uptake in subsequent phases are controlled by diffusion inside meso- and micropores (Almahri et al., 2023). The variance in adsorption energies between adsorptive sites, which is directly related to their heterogeneous nature, was further clarified by introducing the Elovich equation. With respect to TZ, Table S4 predicted initial adsorption (α) and desorption (β) rates of 0.46 and 0.47 $g \cdot mmol^{-1}$ amply illustrated Tb-remarkable MOF's efficacy (Al-Hazmi et al., 2022).

3.6. Adsorption thermodynamics

The ability of tartrazine (TZ) to bind to Tb-MOF is expected to be influenced by temperature. Temperature-dependent improvements in the MOF's adsorption capacity are common since the adsorption process is an endothermic reaction. The properties of the adsorbate and the MOF, the concentration of the adsorbate, and the experimental design will determine the precise influence of temperature on tartrazine adsorption on Tb-MOF (El-Desouky et al., 2021).

The equilibrium constant (K_{eq}), which is connected to the adsorption capacity of the MOF, can be utilized to quantify the temperature dependence of an adsorption process using the Van't Hoff equation. ΔH°_{ads} , R, and T stand for the enthalpy of adsorption, the gas constant, and the absolute temperature, respectively (Fig. 6(a)). Based on the equilibrium constant's temperature dependence, the Van't Hoff equation can be used to calculate the enthalpy of adsorption (El-Desouky

et al., 2021). The enthalpy of adsorption model, which can be used to explain how temperature affects the rate of adsorption, can be used to calculate the effect of temperature on tartrazine adsorption on Tb-MOF.

Thermodynamic characteristics were calculated using adsorption data at different temperatures, including the change in enthalpy (ΔH°), change in free Gibbs energy (ΔG°), and change in entropy (ΔS°) to gain a deeper comprehension of the TZ dye adsorption process onto the Tb-MOF surface, refer to Fig. 6(b). It is clear that adsorption is more advantageous at higher temperatures since the negative values of ΔG° diminish with temperature (288 to 318 K). The endothermic nature of the adsorption process is indicated by the positive ΔH° values. Additionally, the positive ΔS° shows that the degrees of freedom at the solid-liquid interface increase by $387.7 \text{ J} \cdot \text{mol}^{-1} \cdot \text{K}^{-1}$ as the dye is adsorbed onto the Tb-MOF (Tables S8 and S9). These data's ΔH° value for 108.9 kJ/mol generally indicated that the adsorption process was endothermic, meaning that it expanded in tandem with temperature (El-Metwaly et al., 2022).

3.7. Mechanism of interaction

TZ's adsorption on Tb-MOF adsorbents is controlled by a variety of interplay mechanisms. For effective methods of eliminating the color from water and wastewater, it is imperative to comprehend these mechanisms. Optimizing the adsorption conditions and choosing the right adsorbent are essential to maximizing the effectiveness of the color removal process. For the procedure to be effective, its physical-chemical

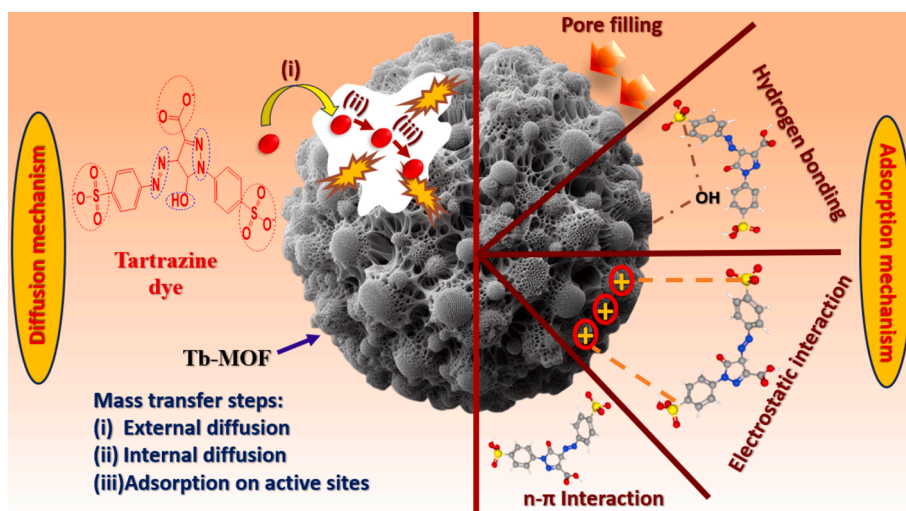


Fig. 7. Mechanism of interaction and diffusion mechanism of TZ onto Tb-MOF.

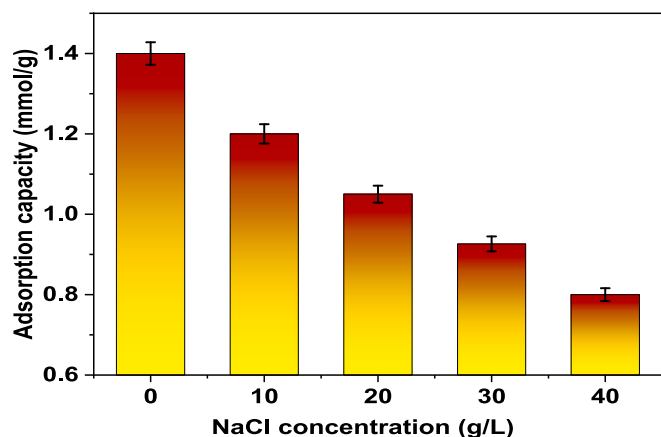


Fig. 8. TZ adsorption onto Tb-MOF and the effect of NaCl. (C_0 : 1.556×10^{-3} mmol, time: 100 min., dose: 0.02 g, volume: 25 mL, agitation speed 180 rpm, NaCl (0 to 40 g/L) and temp.: 25 °C).

parameters pH, dye concentration, dosage of the adsorbent, temperature, contact time, and adsorbent particle size must be optimized. Fig. 7 illustrates the main possible adsorption sites between adsorbents and the TZ chemical structure using different intermolecular interactions. It shows the most likely proteolytic structure for a neutral pH media, with the sulfonate and carboxylate groups highlighted in red and accessible for possible electrostatic interactions with charged adsorbents. The groups that form hydrogen bonds with the adsorbents are indicated in blue. Additionally, as the molecular structure of TZ shows (Fig. 7). Interactions between π and π stacking are conceivable because of the molecule's massive π electronic system, especially with the aromatic rings. The main mechanism for TZ adsorption on Tb-MOF is electrostatic interactions between dye charges and adsorbent surface charges. Functional groups in Tb-MOF, such as amino acids, can enhance adsorption by forming hydrogen bonds. Conversely, because of its porous surface and electrostatic characteristics, Tb-MOF is renowned for having a high adsorption capacity. Van der Waals interactions and π - π stacking between dye molecules and the Tb-MOF surface promote TZ adsorption on activated carbon. A high TZ adsorption capacity is also exhibited by metal organic framework materials functionalized with specific chemical groups, such as amines and hydroxyls, through hydrogen bonding and electrostatic interactions (Al-Hazmi et al., 2022; Alsuhaibani et al., 2022; Al-Hazmi et al., 2022).

3.8. Effect of ionic strength (addition of NaCl) and real sample application

A concentration of NaCl (C_0 : 1.36×10^{-3} mmol.L⁻¹; sorbent dosage: 0.02 g/25 mL) was applied in order to examine the effect of chloride ions

on TZ extraction. The sorption efficacy decreases with increasing NaCl concentration in the adsorbents. The absorption capacity was lowered by 20 % at a sodium chloride concentration of 20 g/L. This might be as a result of the chloride anions' conflicting influence on the TZ cations' ability to interact with the sorption sites. Even at a NaCl concentration of 40 g.L⁻¹, the adsorption efficiency decreases by 1.5 %, indicating that the potential is preserved even in harsh circumstances (Fig. 8) (Mohamed et al., 2021). A number of real water samples, including tap water, sea water, and industrial effluent, were examined to determine the Tb-MOF removal efficacy of TZ dye. The percentages of TZ dye (100 mg/L) concentration were used to determine the removal percentages for tap water based on the second run, while the percentages for sea and waste water were based on the third run 94.4, 92.6 and 88.6 % for tap water, sea water and wastewater, respectively. The results of this study confirm that the Tb-MOF has a high capacity to remove the investigated anionic dye from water, which supports the adsorbent's possible usage in water remediation (Kusuma et al., 2022; Kusuma et al., 2018).

3.9. Reusability

Recyclability is a critical factor in the commercialization of freshly synthesized adsorbent materials since it is directly related to the cost-effectiveness of the adsorption processes. Additionally, the complete regeneration and recyclable nature of the utilized adsorbent materials improve environmental purity and lessen disposal problems (El-Desouky et al., 2022; El-Bindary et al., 2022). The recyclability of Tb-MOF particles was therefore investigated after the spent MOF particles were repeatedly cleaned with diluted NaOH and ethanol solutions. Fig. 9(a) shows that the adsorption efficiency of this adsorbent toward TZ molecules does not drop dramatically with an increase in the number of adsorptions-desorption cycles, indicating that this MOF can be recovered several times without notably losing adsorption capability. Because of this, this MOF's adsorption ability toward TZ molecules continues to be quite strong even after six rounds of adsorption and desorption, albeit at a rate that is about 15 % lower than that of Tb-MOF particles. We may therefore conclude that the produced Tb-MOF particles would be a good option for removing TZ from water (El-Desouky et al., 2022; Al-Wasidi et al., 2022). The other important consideration for commercialization and industrial applications of adsorbent materials is their structural stability. In order to do this, the regenerated Tb-MOF particles were subjected to XRD examination. As shown in Fig. 9(b), all of the characteristic XRD peaks of the Tb-MOF particles remained unchanged, suggesting that the crystalline structure of this MOF was successfully maintained even after six cycles of adsorption and desorption (Kiwaan et al., 2021; Al-Hazmi et al., 2022; Alsuhaibani et al., 2022).

3.11. Comparison with other adsorbents

The Langmuir monolayers have an adsorption capacity of 817.63

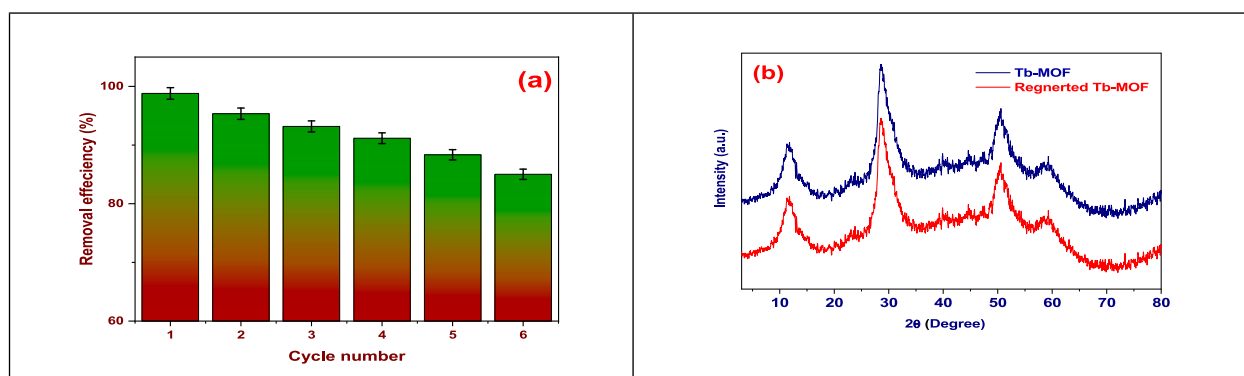


Fig. 9. (a) Efficiency of adsorption TZ onto Tb-MOF, and (b) XRD pattern of Tb-MOF and regenerated.

Table 1

Results for TZ's adsorption capacity and response surface central composite design.

Run	Actual variables			Yield (mmol/g)		
	Dose	Time (min.)	pH	Experimental	Predicted	Residue
1	0.135	52.5	7	1.03	1.03	0.0000
2	0.25	5	7	0.3640	0.3605	0.0035
3	0.02	100	7	1.42	1.42	-0.0035
4	0.135	52.5	7	1.03	1.03	0.0000
5	0.02	5	7	0.3770	0.3902	-0.0132
6	0.135	100	12	1.31	1.31	0.0054
7	0.25	100	7	1.37	1.35	0.0132
8	0.25	52.5	2	1.03	1.03	0.0018
9	0.02	52.5	2	1.13	1.11	0.0186
10	0.135	52.5	7	1.03	1.03	0.0000
11	0.25	52.5	12	0.9547	0.9733	-0.0186
12	0.135	52.5	7	1.03	1.03	0.0000
13	0.135	5	2	0.3774	0.3828	-0.0054
14	0.135	52.5	7	1.03	1.03	0.0000
15	0.135	5	12	0.3499	0.3349	0.0150
16	0.135	100	2	1.42	1.43	-0.0150
17	0.02	52.5	12	0.9870	0.9888	-0.0018

Table 2

Variance analysis for the models that were fitted.

Source	Sum of squares	Df	Mean squares	F-value	P-value
Model	2.17	9	0.2406	1064.95	< 0.0001 significant
A-Dose	0.0046	1	0.0046	20.40	0.0027
B-time	2.04	1	2.04	9040.19	< 0.0001
C-pH	0.0147	1	0.0147	65.16	< 0.0001
AB	0.0003	1	0.0003	1.48	0.2637
AC	0.0011	1	0.0011	4.66	0.0678
BC	0.0014	1	0.0014	6.35	0.0398
A ²	0.0002	1	0.0002	0.7262	0.4223
B ²	0.0994	1	0.0994	439.83	< 0.0001
C ²	0.0004	1	0.0004	1.97	0.2031
Residual	0.0016	7	0.0002		
Lack of Fit	0.0016	3	0.0005		
Pure Error	0.0000	4	0.0000		
Cor Total	2.17	16			

mg/g. Table S10 presents the comparison of TZ's adsorption capability with other adsorbents in the current experiment. When compared to other well-known adsorbents, the Tb-MOF was shown to have a noticeably higher capacity for TZ adsorption (Mittal et al., 2007; Mittal et al., 2006). On the other hand, because TZ exhibits high adsorption in our investigations for all of the adsorbents indicated in Table S10, Tb-MOF can be utilized directly for TZ wastewater treatment without causing additional costs or environmental issues (El-Metwaly et al., 2022; Putri et al., 2019).

Table 3

A statistical overview of many models.

Source	Std. Dev.	Sequential p-value	Lack of Fit p-value	Press	Adj R ²	Pred R ²	Remark
Linear	0.0900	< 0.0001	< 0.0001	0.1937	0.9402	0.9106	
2F1	0.1012	0.9629	< 0.0001	0.4158	0.9244	0.8081	
Quadratic	0.0150	< 0.0001	< 0.0001	0.0253	0.9983	0.9883	Suggested
Cubic	0.0000				1.0000		Aliased

3.12. Statistical analysis

Table 1 presents the results of the RSM analysis that was conducted. The response surface equation's coefficients were calculated using the experimental extraction yields. The least squares method was used to generate the regression coefficients for the intercept, linear, quadratic, and interaction components of the model. Table 2 shows the findings. The resulting Eqs. (7) and (8) were determined to reasonably agree with the Adjusted R² of 0.9983, with a difference of less than 0.2, and to accurately match the Predicted R² of 0.9883. Adeq Precision calculates the ratio of signal to noise. Ideally, the ratio should be higher than 4. With a ratio of 95.102, your signal strength is sufficient. The design area can be navigated with the help of this model (Table 3).

A high R² value suggests that the fluctuation may be well explained by the data fitting the model. Smaller TZ values provide better repeatability because they display the standard deviation as a proportion of the mean. The model demonstrated reproducibility with a coefficient of variation (TZ) below 10. The model had a predicted residual sum of squares (PRESS) of 0.0253, This gauges how well a certain model fits every point in the blueprint. The significance of the model was indicated by its F-value of 1064.95 (Ansori et al., 2019). The model's F-value of 1066.04 indicates that the model is significant. Just 0.01 percent of the time, an F-value this large would result from noise. Model terms with P-values less than 0.0500 are deemed significant. In this case A, B, C, AC, C2 are important terms in the model. If the value is greater than 0.1000, the model terms become irrelevant Eqs. (2) and (3) were represented the coded and actual formula as the follow:

Coded formula;

$$q_e = 1.028 - 0.0240025xA + 0.505279xB - 0.0428988xC - 0.0091325xAB + 0.0162225xAC - 0.01894xBC + 0.0062425xA^2 - 0.153625xB^2 - 0.010285xC^2 \quad (2)$$

Actual formula;

$$qe = 0.344049 - 0.445883xDose + 0.0185707xTime - 0.00244217xpH - 0.00167185xDoseTime + 0.028213xDosepH - 7.97474E - 05xTimepH + 0.472023xDose^2 + - 6.80886E - 05xTime^2 - 0.0004114xpH^2 \quad (3)$$

3.13. Perturbation plot

Plots of perturbations compare all the variables at a given position in the design space. Fig. 10(a) displays the perturbation plot for the Tb-capacity MOFs to adsorb TZ. One element was changed across its range to determine the yield response, while all other parameters remained unchanged. The plot shows how each component has an impact on a key location inside the design area (Time, Dose, and pH). The ability for adsorption seems to be positively impacted by every factor. Time, pH, and dose all had a considerable impact on the curvature effect, as shown by the perturbation Fig. 10(a). The measurements of pH and dose taken during the adsorption process showed how quickly these variables had an impact on the adsorption capacity. The determined adsorption capacity response was positively impacted by the adsorption process's duration, pH, and dosage (Kusuma et al., 2022).

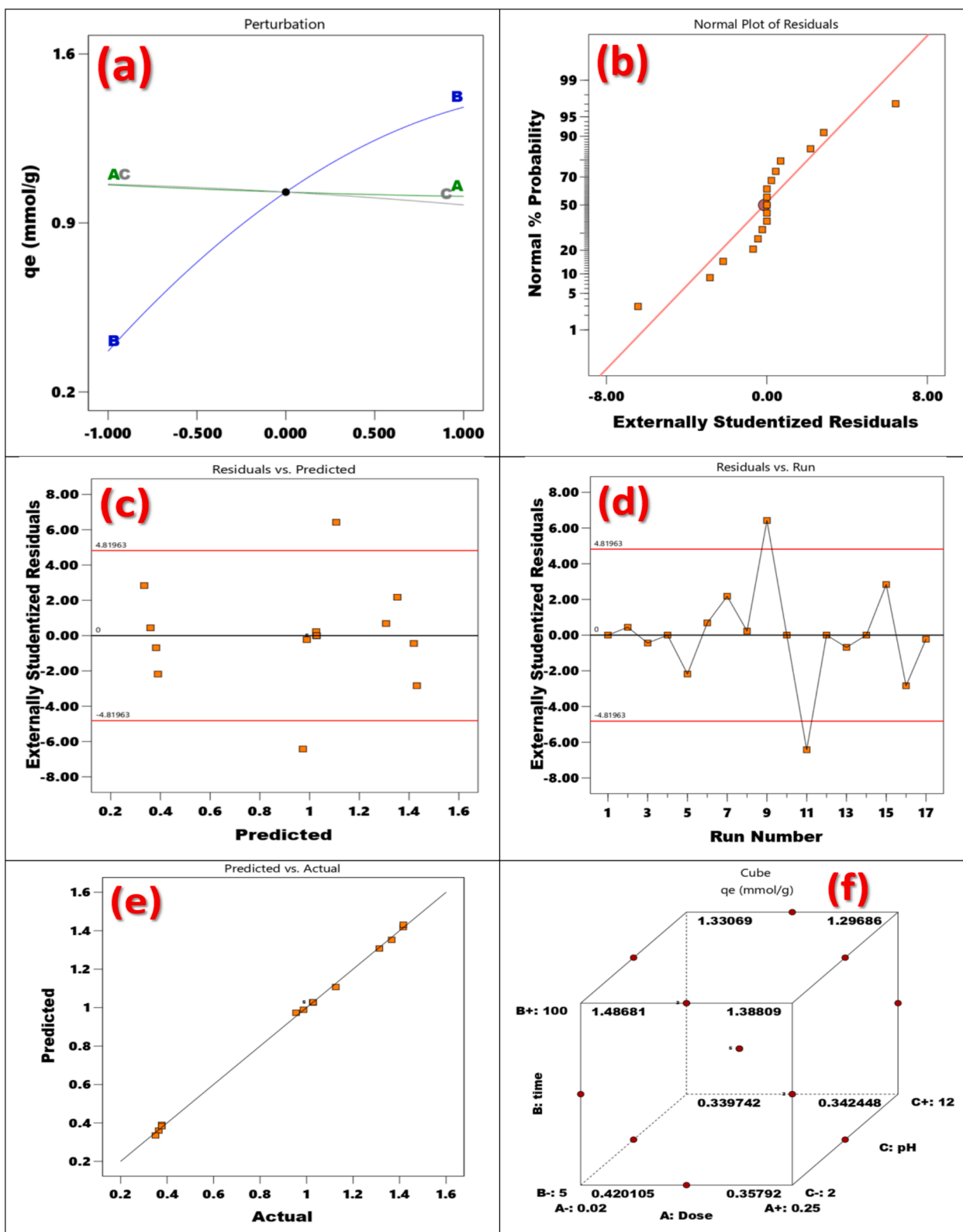


Fig. 10. (a) Perturbation of adsorption TZ onto Tb-MOF, (b) Normal plot of residuals vs. Normal % probability, (c) plot of residuals vs. the predicted response with externally studentized residual, (d) residuals vs. run with externally studentized residual, (e) Predicted vs. Actual with predicted, and (f) Graphical optimization of adsorption capacity of TZ onto Tb-MOF.

3.14. Model adequacy checking

Verifying that the fitted model adequately represents the actual system is typically crucial. Insufficient or inaccurate results may arise

from the analysis and optimization of the fitted response surface if the model does not exhibit a good match. The residuals from the least squares fit are crucial for determining whether a model is adequate. To test the normality assumption, a normal probability map of the residuals

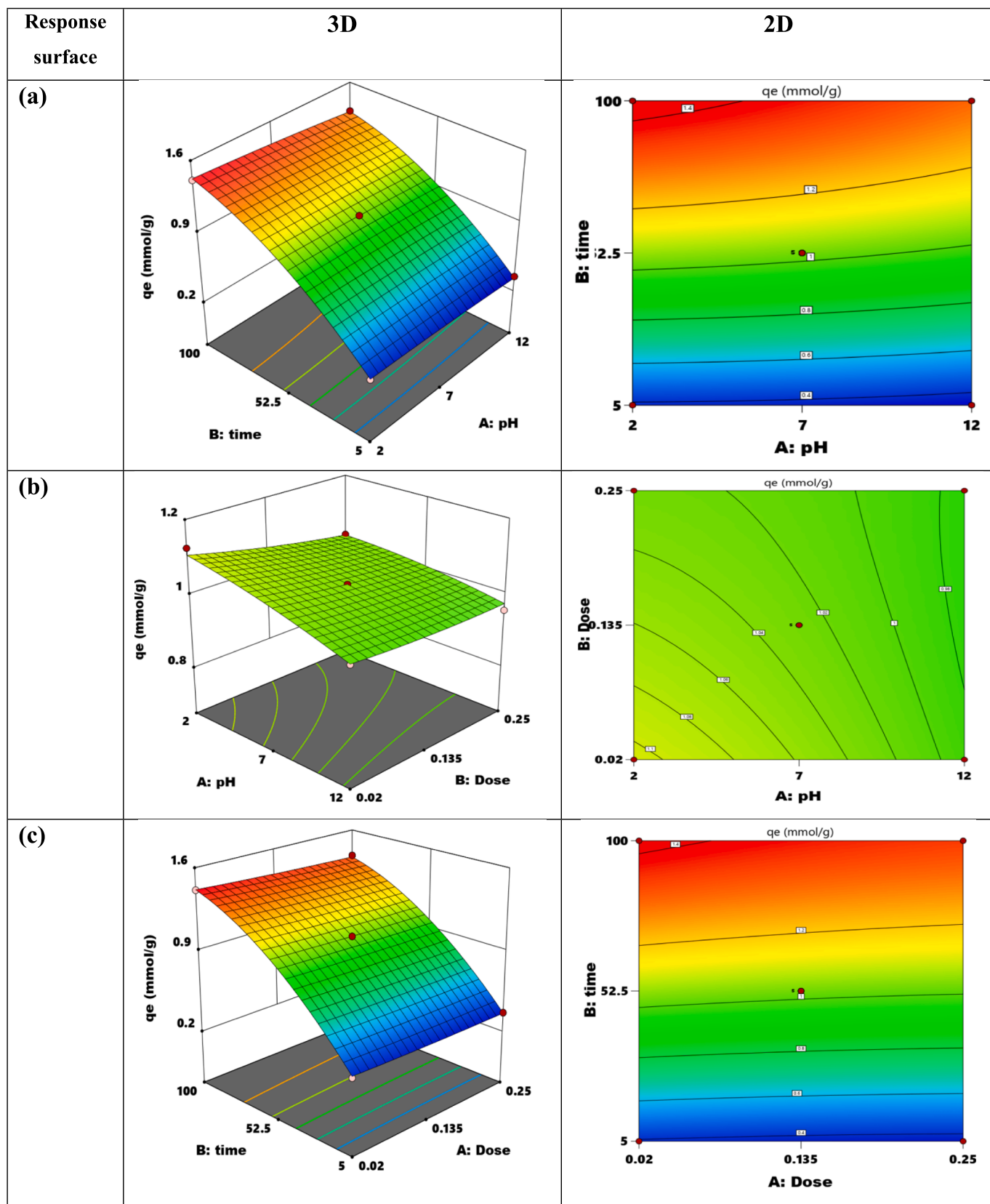


Fig. 11. Response surface (3-D) and 2D.

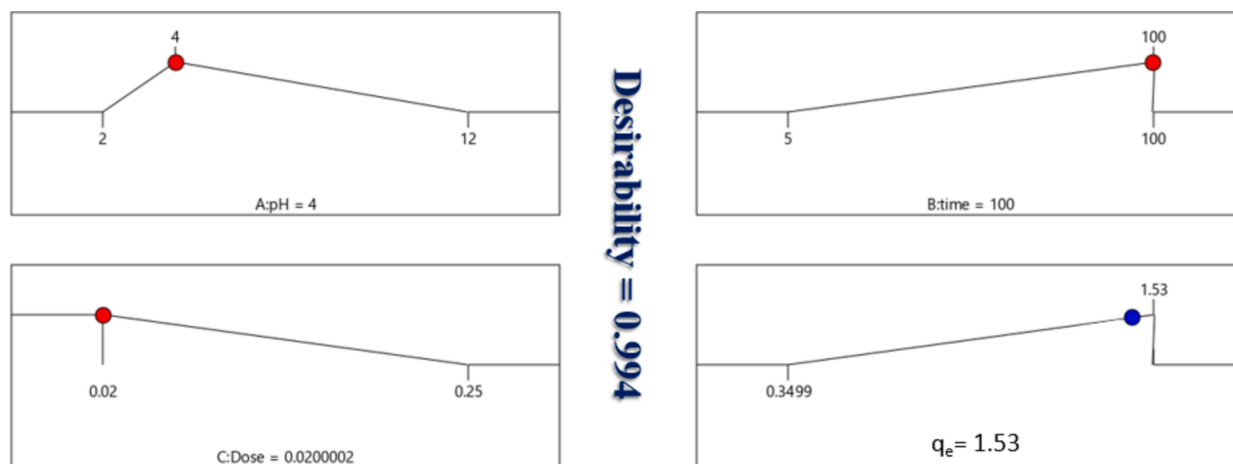


Fig. 12. For TZ removal, response and desirability functions are anticipated.

was created, as shown in Fig. 10(b). The residual plot satisfied the normality requirement because it generally followed a straight line. A much studentized residuals graphic showing the residuals vs. the anticipated values Fig. 10(c). Plot residual versus highly studentized residuals run Fig. 10(d). The normality assumption was verified by mapping the normal probability of the residuals, as shown in Fig. 10(e). In conclusion, the optimal conditions for TZ adsorption onto Tb-MOF are pH 4, 100 min, and a dosage of 0.02 g (Fig. 10(f)). In this optimal state, the predicted adsorption capacity was 1.53 mmol/g (Kusuma et al., 2015).

3.15. Optimization of adsorption of TZ onto Tb-MOF

Plotting the equation's response surface was the most effective method of illuminating how each parameter affected the adsorption capacity within the experimental region under study (Kusuma et al., 2018). Design-Expert software (version 9.0.4.1) was used to plot response surfaces in order to study the effects of various factors and how they interacted with the adsorption capacity. Fig. 11 shows the adsorption capacity values as a function of time, dose, and pH.

When the contour plot and the three-dimensional response surface plot for the adsorption capacity with changing pH and time were made in Fig. 11(a). The ideal adsorption conditions are found in an acidic medium with a pH of 4 and a duration of one hundred minutes. It was evident that as time and pH decreased, the adsorption capacity increased. The adsorption capacity was 1.53 mmol/g (Kusuma and Mahfud, 2015).

When the contour plot and the three-dimensional response surface plot for the adsorption capacity with different times and doses ranging from 0.02 to 0.25 g were made in Fig. 11(b). It is clear that as the adsorbent dose is decreased, the adsorption capacity rises. As time goes on, the adsorption capacity likewise rises (Mogharbel et al., 2024; Kusuma et al., 2015). Fig. 11(c) shows how time and dose affect the amount of adsorption capacity. When pH falls, adsorption capacity rises, peaking at pH 4, where adsorption capacity is greatest. On the other hand, adsorption capacity rises with increased contact time. It is concluded that pH 4, period of 100 min, and dose of 0.02 g are the ideal TZ adsorption conditions onto Tb-MOF. The estimated adsorption capacity at this optimum setting was 1.53 mmol/g.

3.16. Validation of the model

Tb-MOF was employed in Fig. 12 at a dose of 0.02 to 0.25 g, with an interaction period of 5 to 100 min and a pH range of 2 to 12. For acetaminophen to adsorb onto Tb-MOF, the following parameters were optimal: pH 4, 0.02 g of adsorbent, and 100 min of contact time. The

results of the experiment agree with the expected answers rather well. This demonstrated that the model was suitable and sufficient.

4. Conclusion

The metal-organic frameworks of terbium with 2-methyl imidazole were built using batch experiments and the solvothermal technique. Through the use of XRD, XPS, BET, and FT-IR techniques, the adsorbent was characterized. The sorbents have a pH_{PZC} of 5.36, which indicates that they will be protonated in acidic solutions, according to the point of zero charge analysis. The kinetic analysis revealed that the adsorption of TZ dye over Tb-MOF was consistent with pseudo-second-order and Langmuir isotherms. It was discovered that the temperature had an endothermic, spontaneous effect on the adsorption process. More research was done on the efficacy of regeneration, and the outcomes showed success for more than five cycles. Additionally, the effects of dealing with real samples were examined using Box-Behnken Design optimization (BBD). Lastly, thorough uptake kinetics testing has produced encouraging outcomes for the TZ dye's adsorption onto Tb-MOF. This nanocomposite's efficacy has been compared to other materials and well-known adsorbents in order to throw light on its advantages. The existing materials and process system offers incredible prospects for environmental management. In an effort to preserve the environment, research must be done to find newer, more potent, and effective nanomaterials for multifunctional use given the large expansion of polluted wastewater constituted of non-biodegradable dyes and other biological matter.

Statement of data availability

The text contains all necessary information, which is also available upon request via the corresponding author.

Author contributions

All the authors contributed equally to this work.

CRediT authorship contribution statement

Omaymah Alaysuy: Writing – original draft, Visualization, Software, Resources. **Abdullah Ali A. Sari:** Writing – original draft, Validation, Methodology, Formal analysis. **Albandary Almahri:** Writing – original draft, Software, Resources, Methodology. **Kamelah S. Alrashdi:** Writing – original draft, Resources, Methodology, Investigation. **Ibrahim S.S. Alatawi:** Writing – original draft, Visualization, Methodology, Formal analysis. **Meshari M. Aljohani:** Writing – original

draft, Visualization, Methodology, Formal analysis. **Ali Sayqal**: Writing – original draft, Methodology, Formal analysis, Data curation. **Nashwa M. El-Metwaly**: Writing – review & editing, Supervision, Project administration.

Declaration of competing interest

The authors declare that they have no known competing financial interests or personal relationships that could have appeared to influence the work reported in this paper.

Appendix A. Supplementary data

Supplementary data to this article can be found online at <https://doi.org/10.1016/j.arabjc.2024.106035>.

References

- Abd El-Wahab, M., El-Desouky, M.G., 2022. Study the effect of antioxidants on biological activity and on homopolypyrrolene; mechanical and physical properties. *J. Indian Chem. Soc.* 99, 100764.
- Alaysuy, O., Aljohani, M.M., Alkhamis, K., Alatawi, N.M., Almotairy, A.R.Z., Abu Al-Ola, K.A., Khder, A.S., El-Metwaly, N.M., 2024. Synthesis, characterization and adsorption optimization of bimetallic La–Zn metal organic framework for removal of 2,4-dichlorophenylacetic acid. *Heliyon* 10, e28622.
- Al-Hazmi, G.H., Adam, A.M.A., El-Desouky, M.G., El-Bindary, A.A., Alsuhaibani, A.M., Refat, M.S., 2023. Efficient adsorption of rhodamine b using a composite OF Fe₃O₄@ZIF-8: Synthesis, Characterization, modeling analysis, statistical physics and mechanism of interaction. *Bull. Chem. Soc. Ethiop.* 37, 211–229.
- Al-Hazmi, G.A.A.M., Alayyafi, A.A., El-Desouky, M.G., El-Bindary, A.A., 2024. Chitosan-nano CuO composite for removal of mercury (II): Box-Behnken design optimization and adsorption mechanism. *Int. J. Biol. Macromol.* 261, 129769.
- Al-Hazmi, G.A.A.M., Alayyafi, A.A., El-Desouky, M.G., El-Bindary, A.A., 2024. Guava seed activated carbon loaded calcium alginate aerogel for the adsorption of diclofenac sodium: Characterization, isotherm, kinetics, and optimization via Box-Behnken design. *Int. J. Biol. Macromol.* 262, 129995.
- Al-Hazmi, G.A.A., El-Bindary, M.A., El-Desouky, M.G., El-Bindary, A.A., 2022. Efficient adsorptive removal of industrial dye from aqueous solution by synthesized zeolitic imidazolate framework-8 loaded date seed activated carbon and statistical physics modeling. *Desalin. Water Treat.* 258, 85–103.
- Al-Hazmi, G.A.A., El-Zahhar, A.A., El-Desouky, M.G., El-Bindary, A., 2024. Superior adsorption and removal of doxorubicin from aqueous solution using activated carbon via thermally treated green adsorbent: isothermal, kinetic, and thermodynamic studies. *Environ. Technol. (United Kingdom)* 45, 1969–1988.
- Al-Hazmi, G.A.A., El-Zahhar, A.A., El-Desouky, M.G., El-Bindary, M.A., El-Bindary, A.A., 2024. Efficiency of Fe₃O₄@ZIF-8 for the removal of Doxorubicin from aqueous solutions: equilibrium, kinetics and thermodynamic studies. *Environ. Technol. (United Kingdom)* 45, 731–750.
- Al-Hazmi, G.H., Refat, M.S., El-Desouky, M.G., El-Bindary, A.A., 2022. Effective adsorption and removal of industrial dye from aqueous solution using mesoporous zinc oxide nanoparticles via metal organic framework: equilibrium, kinetics and thermodynamic studies. *Desalin. Water Treat.* 272, 277–289.
- Al-Hazmi, G.H., Refat, M.S., El-Desouky, M.G., Wali, F.K.M., El-Bindary, A.A., 2022. Effective removal of industrial dye from aqueous solution using mesoporous nickel oxide: a complete batch system evaluation. *Desalin. Water Treat.* 273, 246–260.
- Aljohani, M.M., Al-Qahtani, S.D., Alshareef, M., El-Desouky, M.G., El-Bindary, A.A., El-Metwaly, N.M., El-Bindary, M.A., 2023. Highly efficient adsorption and removal bio-staining dye from industrial wastewater onto mesoporous Ag-MOFs. *Process Saf. Environ. Prot.* 172, 395–407.
- Alluhaybi, A.A., Alharbi, A., Alshammari, K.F., El-Desouky, M.G., 2023. Efficient adsorption and removal of the herbicide 2,4-dichlorophenylacetic acid from aqueous solutions using ML-88(Fe)-NH₂. *ACS Omega* 8, 40775–40784.
- Almahri, A., Morad, M., Aljohani, M.M., Alatawi, N.M., Saad, F.A., Abumelha, H.M., El-Desouky, M.G., El-Bindary, A.A., 2023. Atrazine reclamation from an aqueous environment using a ruthenium-based metal-organic framework. *Process Saf. Environ. Prot.* 177, 52–68.
- Almahri, A., Abou-Melha, K.S., Katouah, H.A., Al-bonayan, A.M., Saad, F.A., El-Desouky, M.G., El-Bindary, A.A., 2023. Adsorption and removal of the harmful pesticide 2,4-dichlorophenylacetic acid from an aqueous environment via coffee waste biochar: Synthesis, characterization, adsorption study and optimization via Box-Behnken design. *J. Mol. Struct.* 1293, 136238.
- Almahri, A., El-Metwaly, N.M., 2024. Enhancing methyl violet 2B pollutant removal from wastewater using Al-MOF encapsulated with poly (itaconic acid) grafted crosslinked chitosan composite sponge: Synthesis, characterization, DFT calculation, adsorption optimization via box-behnken design. *Int. J. Biol. Macromol.* 276, 133909.
- Al-Qahtani, S.D., Alhasani, M., Alkathami, N., Abu Al-Ola, K.A., Alkhamis, K., El-Desouky, M.G., El-Bindary, A.A., 2023. Effective levofloxacin adsorption and removal from aqueous solution onto tea waste biochar; synthesis, characterization, adsorption studies, and optimization by Box-Behnken design and its antibacterial activity. *Environ. Technol. (United Kingdom)* 45, 4928–4950.
- Alrefae, S.H., Aljohani, M., Alkhamis, K., Shaaban, F., El-Desouky, M.G., El-Bindary, A.A., El-Bindary, M.A., 2023. Adsorption and effective removal of organophosphorus pesticides from aqueous solution via novel metal-organic framework: adsorption isotherms, kinetics, and optimization via Box-Behnken design. *J. Mol. Liq.* 384, 122206.
- Alsharief, H.H., Alatawi, N.M., Al-bonayan, A.M., Alrefae, S.H., Saad, F.A., El-Desouky, M.G., El-Bindary, A.A., 2024. Adsorption of Azorubine E122 dye via Namordenite with tryptophan composite: batch adsorption, Box-Behnken design optimisation and antibacterial activity. *Environmental Technology (United Kingdom)* 45, 3496–3515.
- Alsuhaibani, A.M., Refat, M.S., Atta, A.A., El-Desouky, M.G., El-Bindary, A.A., 2022. Efficient adsorption and removal of tetracycline antibiotics from aqueous solutions onto nickel oxide nanoparticles via organometallic chelate. *Desalin. Water Treat.* 277, 190–205.
- Alsuhaibani, A.M., Refat, M.S., Adam, A.M.A., El-Desouky, M.G., El-Bindary, A.A., 2023. Enhanced adsorption of ceftriaxone antibiotics from water by mesoporous copper oxide nanosphere. *Desalin. Water Treat.* 281, 234–248.
- Alsuhaibani, A.M., Alayyafi, A.A., Albedair, L.A., El-Desouky, M.G., El-Bindary, A.A., 2024. Synthesis and characterization of metal-organic frameworks based on thorium for the effective removal of 2, 4-dichlorophenylacetic pesticide from water: Batch adsorption and Box-Behnken Design optimization, and evaluation of reusability. *J. Mol. Liq.* 398, 124252.
- Al-Wasidi, A.S., AlZahrani, I.I.S., Thawbaraka, H.I., Naglah, A.M., El-Desouky, M.G., El-Bindary, M.A., 2022. Adsorption studies of carbon dioxide and anionic dye on green adsorbent. *J. Mol. Struct.* 1250, 131736.
- Ansari, R., Banimahd Keivani, M., Fallah Delavar, A., 2011. Application of polyaniline nanolayer composite for removal of tartrazine dye from aqueous solutions. *J. Polym. Res.* 18, 1931–1939.
- Ansori, A., Wibowo, S.A., Kusuma, H.S., Bhuana, D.S., Mahfud, M., 2019. Production of biodiesel from nyamplung (*Calophyllum inophyllum* L.) using microwave with CaO catalyst from eggshell waste: optimization of transesterification process parameters. *Open Chem.* 17, 1185–1197.
- Arora, C., Soni, S., Bajpai, P., Mittal, J., Mariyam, A., 2021. Dye removal from waste water using metal organic frameworks, Management of Contaminants of Emerging Concern (CEC). *Environ.* 375, 375–394.
- Dhar, A., Ruprecht, H., Klumpp, R., Vacik, H., 2007. Comparison of ecological condition and conservation status of English yew population in two Austrian gene conservation forests. *J. for. Res.* 18, 181–186.
- Dubinina, M., 1947. The equation of the characteristic curve of activated charcoal. *Proc. Acad. Sci. USSR, Phys. Chem. Sect.* 55, 327–329.
- Dutta, P., Arora, C., Soni, S., Rai, N., Mittal, J., 2022. Metal-organic frameworks for detection and adsorptive removal of pesticides. *Elsevier, Sustainable Materials for Sensing and Remediation of Noxious Pollutants*, pp. 329–340.
- El-Bindary, M.A., El-Desouky, M.G., El-Bindary, A.A., 2022. Metal-organic frameworks encapsulated with an anticancer compound as drug delivery system: synthesis, characterization, antioxidant, anticancer, antibacterial, and molecular docking investigation. *Appl. Organomet. Chem.* 36.
- El-Desouky, M.G., Hassan, N., Shahat, A., El-Didamony, A., El-Bindary, A.A., 2021. Synthesis and characterization of porous magnetite nanosphere iron oxide as a novel adsorbent of anionic dyes removal from aqueous solution. *Biointerface Res. Appl. Chem.* 11, 13377–13401.
- El-Desouky, M.G., El-Bindary, M.A., El-Bindary, A.A., 2021. Effective adsorptive removal of anionic dyes from aqueous solution, Vietnam. *J. Chem.* 59, 341–361.
- El-Desouky, M.G., Abd El-Wahab, M., El-Bindary, A.A., 2022. Interpretations and DFT calculations for polypropylene/copper oxide nanosphere, *Biointerface Research in Applied Chemistry* 12, 1134–1147.
- El-Desouky, M.G., El-Bindary, A.A., El-Bindary, M.A., 2022. Low-temperature adsorption study of carbon dioxide on porous magnetite nanospheres iron oxide, *Biointerface Research in Applied Chemistry* 12, 6252–6268.
- El-Desouky, M.G., Khalil, M.A.G., El-Affify, M.A.M., El-Bindary, A.A., El-Bindary, M.A., 2022. Effective methods for removing different types of dyes – modelling analysis/statistical physics treatment and DFT calculations: a review. *Desalin. Water Treat.* 280, 89–127.
- El-Desouky, M.G., El-Bindary, A.A., El-Affify, M.A.M., Hassan, N., 2022. Synthesis, characterization, theoretical calculation, DNA binding, molecular docking, anticovid-19 and anticancer chelation studies of some transition metal complexes, *Inorganic and Nano-Metal Chemistry* 52, 1273–1288.
- El-Desouky, M.G., Khalil, M.A., El-Bindary, A.A., El-Bindary, M.A., 2022. Biological, biochemical and thermochemical techniques for biofuel production: An updated review. *Biointerface Res. Appl. Chem.* 12, 3034–3054.
- El-Desouky, M.G., Shahat, A., El-Bindary, A.A., El-Bindary, M.A., 2022. Description, kinetic and equilibrium studies of the adsorption of carbon dioxide in mesoporous iron oxide nanospheres. *Biointerface Res. Appl. Chem.* 12, 1022–1038.
- El-Fattah, W.A., Guesmi, A., Ben Hamadi, N., El-Desouky, M.G., Shahat, A., 2024. A green synthesis of cellulose nanocrystals biosorbent for remediation of wastewater containing industrial dye. *Colloids Surf A Physicochem Eng Asp* 681, 132729.
- El-Metwaly, N.M., Katouah, H.A., El-Desouky, M.G., El-Bindary, A.A., El-Bindary, M.A., 2022. Fabricating of Fe₃O₄@Ag-MOF nanocomposite and evaluating its adsorption activity for removal of doxorubicin. *J. Environ. Sci. Health - Part A Toxic/Hazardous Substances Environ. Eng.* 57, 1099–1115.
- Fernández-Andrade, K.J., González-Vargas, M.C., Rodríguez-Rico, I.L., Ruiz-Reyes, E., Quiroz-Fernández, L.S., Baquerizo-Crespo, R.J., Rodríguez-Díaz, J.M., 2022. Evaluation of mass transfer in packed column for competitive adsorption of Tartrazine and brilliant blue FCF: a statistical analysis. *Results Eng.* 14, 100449.

- Fiorito, S., Epifano, F., Palumbo, L., Collevicchio, C., Spogli, R., Genovese, S., 2023. Separation and quantification of Tartrazine (E102) and Brilliant Blue FCF (E133) in green colored foods and beverages. *Food Res. Int.* 172, 113094.
- Freundlich, H.M.F., 1906. Over the adsorption in solution. *J. Phys. Chem.* 57, 385–471.
- Gamoudi, S., Srasra, E., 2019. Adsorption of organic dyes by HDPy+-modified clay: effect of molecular structure on the adsorption. *J. Mol. Struct.* 1193, 522–531.
- Gaur, B., Mittal, J., Shah, S.A.A., Mittal, A., Baker, R.T., 2024. Sequestration of an azo dye by a potential biosorbent: characterization of biosorbent, adsorption isotherm and adsorption kinetic studies. *Molecules* 29, 2387.
- Gautam, R.K., Gautam, P.K., Banerjee, S., Rawat, V., Soni, S., Sharma, S.K., Chattopadhyaya, M.C., 2015. Removal of tartrazine by activated carbon biosorbents of *Lantana camara*: kinetics, equilibrium modeling and spectroscopic analysis. *J. Environ. Chem. Eng.* 3, 79–88.
- George, A., Cherian, A.R., Jacob, B., Varghese, A., Maiyalagan, T., 2023. Design optimisation and fabrication of amino acid based molecularly imprinted sensor for the selective determination of food additive tartrazine. *Food Chem.* 404, 134673.
- Hassan, N., Shahat, A., El-Didamony, A., El-Desouky, M.G., El-Bindary, A.A., 2020. Equilibrium, kinetic and Thermodynamic studies of adsorption of cationic dyes from aqueous solution using ZIP-8. *Moroccan Journal of Chemistry* 8, 624–635.
- Ho, Y.-S., McKay, G., 1998. Sorption of dye from aqueous solution by peat. *Chem. Eng. J.* 70, 115–124.
- Jain, R., Sharma, P., Sikarwar, S., Mittal, J., Pathak, D., 2014. Adsorption kinetics and thermodynamics of hazardous dye Tropaeoline 000 onto Aeroxide Alu C (Nano alumina): a non-carbon adsorbent. *Desalin. Water Treat.* 52, 7776–7783.
- Joshiba, G.J., Kumar, P.S., Rangasamy, G., Ngeuegni, P.T., Pooja, G., Balji, G.B., Alagumalai, K., El-Serehy, H.A., 2022. Iron doped activated carbon for effective removal of tartrazine and methylene blue dye from the aquatic systems: Kinetics, isotherms, thermodynamics and desorption studies. *Environ. Res.* 215, 114317.
- Kaushal, I., Kumar, V., Saharan, P., Mittal, A., Bhagat, R., Kumar, S., Sharma, A.K., 2023. Electrochemical energy storage and hydrogen peroxide sensing using hybrid framework of CeO₂-MnO₂ on carbon nano fiber composite. *J. Alloy. Compd.* 934, 167740.
- Kiwaan, H.A., Mohamed, F.S., El-Ghamaz, N.A., Beshry, N.M., El-Bindary, A.A., 2021. Experimental and electrical studies of zeolitic imidazolate framework-8 for the adsorption of different dyes. *J. Mol. Liq.* 338, 116670.
- Klett, C., Barry, A., Balti, I., Lelli, P., Schoenstein, F., Jouini, N., 2014. Nickel doped Zinc oxide as a potential sorbent for decolorization of specific dyes, methylorange and tartrazine by adsorption process. *Journal of Environmental. Chem. Eng.* 2, 914–926.
- Kusuma, H.S., Ansori, A., Wibowo, S., Bhuana, D.S., Mahfud, M., 2018. Optimization of transesterification process of biodiesel from Nyamplung (*Calophyllum inophyllum* Linn) using microwave with CaO catalyst. *Korean Chem. Eng. Res.* 56, 435–440.
- Kusuma, H.S., Amenaghawon, A.N., Darmokoeseomo, H., Neolaka, Y.A., Widyaningrum, B.A., Onowise, S.U., Anyalewechi, C.L., 2022. A comparative evaluation of statistical empirical and neural intelligence modeling of *Manihot esculenta*-derived leaves extract for optimized bio-coagulation-flocculation of turbid water. *J. Ind. Crops Products* 186, 115194.
- Kusuma, H.S., Mahfud, M., 2015. Box-Behnken design for investigation of microwave-assisted extraction of patchouli oil. *AIP Conf. Proceed., AIP Publ.*
- Kusuma, H.S., Sudrajat, R.G.M., Susanto, D.F., Gala, S., Mahfud, M., 2015. Response surface methodology (RSM) modeling of microwave-assisted extraction of natural dye from *Swietenia mahagoni*: a comparison between Box-Behnken and central composite design method. *AIP Conf. Proceed., AIP Publ.*
- Lagergren, S.K., 1898. About the theory of so-called adsorption of soluble substances. *Sven. Vetenskapskad. Handlingar* 24, 1–39.
- Langmuir, I., 1916. The constitution and fundamental properties of solids and liquids. Part I. Solids. *J. Am. Chem. Soc.* 38, 2221–2295.
- Mahmoud, M.E., Abdelfattah, A.M., Tharwat, R.M., Nabil, G.M., 2020. Adsorption of negatively charged food tartrazine and sunset yellow dyes onto positively charged triethylenetetramine biochar: Optimization, kinetics and thermodynamic study. *J. Mol. Liq.* 318, 114297.
- Mariyam, A., Mittal, J., Sakina, F., Baker, R.T., Sharma, A.K., 2021. Fixed-bed adsorption of the dye Chrysoidine R on ordered mesoporous carbon. *Desalin. Water Treat.* 229, 395–402.
- Martini, B.K., Daniel, T.G., Corazza, M.Z., de Carvalho, A.E., 2018. Methyl orange and tartrazine yellow adsorption on activated carbon prepared from boiler residue: Kinetics, isotherms, thermodynamics studies and material characterization. *J. Environ. Chem. Eng.* 6, 6669–6679.
- Mittal, J., 2020. Permissible synthetic food dyes in India. *Resonance* 25, 567–577.
- Mittal, A., Kurup, L., Mittal, J., 2007. Freundlich and Langmuir adsorption isotherms and kinetics for the removal of Tartrazine from aqueous solutions using hen feathers. *J. Hazard. Mater.* 146, 243–248.
- Mittal, A., Jain, R., Mittal, J., Varshney, S., Sikarwar, S., 2010. Removal of Yellow ME 7 GL from industrial effluent using electrochemical and adsorption techniques. *Int. J. Environ. Pollut.* 43, 308–323.
- Mittal, J., Mariyam, A., Sakina, F., Baker, R.T., Sharma, A.K., Mittal, A., 2021. Batch and bulk adsorptive removal of anionic dye using metal/halide-free ordered mesoporous carbon as adsorbent. *J. Clean. Prod.* 321, 129060.
- Mittal, J., Ahmad, R., Mariyam, A., Gupta, V., Mittal, A., 2021. Expedient and enhanced sequestration of heavy metal ions from aqueous environment by papaya peel carbon: a green and low-cost adsorbent. *Desalin. Water Treat.* 210, 365–376.
- Mittal, J., Ahmad, R., Mittal, A., 2021. Kahwa tea (*Camellia sinensis*) carbon—a novel and green low-cost adsorbent for the sequestration of titan yellow dye from its aqueous solutions. *Desalin. Water Treat.* 227, 404–411.
- Mittal, A., Mittal, J., Kurup, L., 2006. Adsorption isotherms, kinetics and column operations for the removal of hazardous dye, Tartrazine from aqueous solutions using waste materials—Bottom Ash and De-Oiled Soya, as adsorbents. *J. Hazard. Mater.* 136, 567–578.
- Mogharbel, R.T., Alkhamis, K., Felaly, R., El-Desouky, M.G., El-Bindary, A.A., El-Metwaly, N.M., El-Bindary, M.A., 2024. Superior adsorption and removal of industrial dye from aqueous solution via magnetic silver metal-organic framework nanocomposite. *Environ. Technol. (United Kingdom)* 45, 2558–2574.
- Mohamed, G., Hassan, N., Shahat, A., El-Didamony, A., Ashraf, A., 2021. Synthesis and characterization of porous magnetite nanosphere iron oxide as a novel adsorbent of anionic dyes removal from aqueous solution. *Biointerface Res. Appl. Chem.* 11, 13377–13401.
- Nassef, H.M., Al-Hazmi, G.A.A.M., Alayyafi, A.A., El-Desouky, M.G., El-Bindary, A.A., 2024. Synthesis and characterization of new composite sponge combining of metal-organic framework and chitosan for the elimination of Pb(II), Cu(II) and Cd(II) ions from aqueous solutions: Batch adsorption and optimization using Box-Behnken design. *J. Mol. Liq.* 394, 123741.
- Naushad, M., Ansari, A.A., AlOthman, Z.A., Mittal, J., 2016. Synthesis and characterization of YVO₄: Eu³⁺ nanoparticles: kinetics and isotherm studies for the removal of Cd²⁺ metal ion. *Desalin. Water Treat.* 57, 2081–2088.
- Ouassif, H., Moujahid, E.M., Lahkale, R., Sadik, R., Bouragba, F.Z., Diouri, M., 2020. Zinc-Aluminum layered double hydroxide: High efficient removal by adsorption of tartrazine dye from aqueous solution. *Surf. Interfaces* 18, 100401.
- Patel, A., Soni, S., Mittal, J., Mittal, A., Arora, C., 2021. Sequestration of crystal violet from aqueous solution using ash of black turmeric rhizome. *Desalin. Water Treat.* 220, 342–352.
- Putri, D.K.Y., Dewi, I.E.P., Kusuma, H.S., Mahfud, M., 2019. Extraction of an essential oil from fresh cananga flowers (*Cananga odorata*) using solvent-free microwave method. *J. Chem. Technol. Metall.* 54, 793–802.
- Rai, N., Soni, S., Verma, A., Mittal, A., Baker, R., Shah, S.A.A., Arora, C., 2023. Sequestration of a cationic dye using graphene oxide as adsorbent. *Desalin. Water Treat.* 307, 180–189.
- Ranjbari, S., Ayati, A., Tanhaei, B., Al-Othman, A., Karimi, F., 2022. The surfactant-ionic liquid bi-functionalization of chitosan beads for their adsorption performance improvement toward Tartrazine. *Environ. Res.* 204, 111961.
- Saharan, P., Kumar, V., Kaushal, I., Mittal, A., Shukla, S.K., Kumar, D., Sharma, A.K., Om, H., 2023. A comprehensive review on the metal-based green valorized nanocomposite for the remediation of emerging colored organic waste. *Environ. Sci. Pollut. Res.* 30, 45677–45700.
- Soni, S., Rai, N., Bajpai, P., Mittal, J., Arora, C., 2023. Enhanced sequestration of an acidic dye on novel bimetallic metal-organic framework. *J. Dispers. Sci. Technol.* 45, 107–116.
- Tabrizi, S.H., Tanhaei, B., Ayati, A., Ranjbari, S., 2022. Substantial improvement in the adsorption behavior of montmorillonite toward Tartrazine through hexadecylamine impregnation. *Environ. Res.* 204, 111965.
- Tempkin, V.P.M.I., 1940. Kinetics of ammonia synthesis on promoted iron catalyst. *Acta Phys. Chim. USSR* 12, 327–356.
- Wan Ngah, W.S., Ariff, N.F.M., Hanafiah, M.A.K.M., 2010. Preparation, characterization, and environmental application of crosslinked chitosan-coated bentonite for tartrazine adsorption from aqueous solutions. *Water, Air, Soil Pollution* 206, 225–236.
- Weber Jr, W.J., Morris, J.C., 1963. Kinetics of adsorption on carbon from solution. *J. Sanit. Eng. Div.* 89, 31–59.
- Zhang, L., Sellaoui, L., Franco, D., Dotto, G.L., Bajazhar, A., Belmabrouk, H., Bonilla-Petriciolet, A., Oliveira, M.L., Li, Z., 2020. Adsorption of dyes brilliant blue, sunset yellow and tartrazine from aqueous solution on chitosan: analytical interpretation via multilayer statistical physics model. *Chem. Eng. J.* 382, 122952.